A&A 443, 981–994 (2005)
DOI: 10.1051/0004-6361:20053274

Astronomy & Astrophysics

Electron temperature fluctuations in planetary nebulae⋆

A. C. Krabbe and M. V. F. Copetti

Laboratório de Análise Numérica e Astrofísica, Departamento de Matemática, Universidade Federal de Santa Maria, 97119-900 Santa Maria, RS, Brazil
e-mail: angela@lana.ccne.ufsm.br

Received 20 April 2005 /Accepted 25 July 2005

ABSTRACT

An observational study of the spatial variation of the electron temperature and density in 10 galactic planetary nebulae is presented. The data consist of long-slit spectra of high signal-to-noise ratio in the 3100 to 6900 Å range. Electron temperatures were determined from the [O III](λ 4959 + λ 5007)/λ 4363 and [N II](λ 6548 + λ 6583)/λ 5755 ratios and from the Balmer discontinuity. Electron densities were estimated from the [S II]λ 6716/λ 6731, [Cl III]λ 5517/λ 5537, and [Ar IV]λ 4711/λ 4740 ratios. Electron temperature variations of low amplitude were found across the nebular surface in the planetary nebulae studied. The temperature distribution across each nebula presents a variance relative to the mean corresponding to $0.0003 \leq t^2_s(\mathrm{Bal}) \leq 0.0078$, $0.0003 \leq t^2_s(\mathrm{N\,II}) \leq 0.0097$, and $0.0011 \leq t^2_s(\mathrm{O\,III}) \leq 0.0050$. A systematic spatial variation of electron density has been detected in most of objects (NGC 1535, NGC 2438, NGC 2440, NGC 3132, NGC 3242, NGC 6302, NGC 6563, and NGC 7009). The remaining objects (NGC 6781 and NGC 6853) have not shown any significant electron density dependence on position. NGC 2438, NGC 6563, NGC 6781, and NGC 6853 are in general the most diffuse and probably evolved objects studied here, with low mean densities in the range $N_e(\mathrm{S\,II}) \approx 95$–$158$ cm^{-3}. An anti-correlation between temperature and density was found for NGC 2438 and NGC 3132, with the electron temperature increasing with the decrease of electron density and a correlation between temperature and density was found for NGC 2440, NGC 3242, NGC 6302, and NGC 7009, with the electron temperature increasing with the increase of electron density. These relationships seem to be associated with the structure of the nebula. The nebulae in which the correlation between temperature and density is present are ring shaped. The anti-correlation between temperature and density is found in bipolar planetary nebulae that are denser in the centre of the nebula.

Key words. ISM: planetary nebulae: general

1. Introduction

A fundamental issue that still has not been satisfactorily understood in abundance determinations in planetary nebulae and H II regions is that the abundance of heavy elements derived from their recombination lines are systematically higher than those derived from their collisionally excited emission lines. These discrepancies have been vastly reported in the literature and huge differences have been found. For example, Liu et al. (2000) determined abundances of C, N, O and Ne in the planetary nebula NGC 6153 from recombination lines and found that they are about 10 times higher than those derived from forbidden lines. This difference is even larger, a factor of about 20 times higher, for the galactic bulge planetary nebula M 1–42 (Liu et al. 2001).

One plausible explanation for such discrepancies would be the presence of large internal variation of electron temperature in nebulae. These temperature fluctuations were initially proposed by Peimbert (1967) to explain the considerable differences found between the temperature estimations based on distinct methods in the H II regions M 8, M 17, and the Orion Nebula. However, high values of temperature fluctuations are required to reconcile the abundances derived from recombination and forbidden lines, which are not predicted by standard photoionization models (Kingdon 1995).

Recently, direct determinations of electron temperature fluctuations have been obtained for the planetary nebulae NGC 4361 (Liu 1998) and NGC 7009 (Rubin et al. 2002), and for the H II regions 30 Doradus (Krabbe & Copetti 2002) and Orion Nebula (Rubin et al. 2003; O'Dell et al. 2003) from point-to-point measurements of electron temperature and very low temperature fluctuations have been measured. Up to now these four objects are the only ones for which direct estimations of electron temperature fluctuations have been published. So, observational studies of point-to-point measurements of electron temperature in a larger number of objects are of fundamental importance to estimate the amplitude of temperature fluctuations in gaseous nebulae.

This paper reports a study on the spatial variation of electron temperature and density in 10 galactic planetary nebulae. The electron temperature estimates were derived from point-to-point measurements of the [O III](λ 4959 + λ 5007)/λ 4363

⋆ Figures 5–23 are only available in electronic form at http://www.edpsciences.org

and [N II](λ6548 + λ6583)/λ5755 ratios and from the Balmer discontinuity, obtained from long slit spectrophotometry at high signal-to-noise ratio. Point-to-point measurements of electron densities obtained from the [S II]λ6716/λ6731, [Ar IV]λ4711/λ4740, and [Cl III]λ5517/λ5537 ratios have also been obtained. In a further paper abundances of heavy elements derived from recombination and forbidden lines will be estimated and compared.

2. Observations and reductions

The observations were carried out on January, July and December 2002 with the Boller & Chivens spectrograph attached to the 1.52 m telescope of the European Southern Observatory (ESO), Chile, and on September 1994 and May 2002 with the Cassegrain spectrograph of the 1.6 m telescope at the Laboratório Nacional de Astrofísica (LNA), Brazil. We used a Loral CCD of 2688 × 512 pixels at ESO and at LNA we used a SITe CCD of 1024 × 1024 pixels on May 2002 and an EEV CCD of 800 × 1024 pixels on September 1994. We used a grid of 1200 grooves mm^{-1} at LNA and at ESO we used a grid of 2400 grooves mm^{-1} during the January and July runs and a grid of 1200 grooves mm^{-1} during the December run. The spatial scale was 0.82″ pxl^{-1} for the Loral CCD, 0.90″ pxl^{-1} for the EEV CCD, and 1.0″ pxl^{-1} for the SITe CCD. The slits used have entrances on the plane of sky of 2″ × 250″ for the observations at ESO and 2″ × 320″ for the observations at LNA. Dome flat-field exposures were taken at the beginning and at the end of the nights. Several bias frames were made along each night. Spectrophotometric standard stars were observed for flux calibration. Spectra of a He-Ar-Ne lamp were taken before and after each object exposure for wavelength calibration.

The objects included in this study are listed in Table 1. Multiple spectra with different exposure times were taken at a same slit position in each nebula to increase the signal-to-noise ratio. The exposures times were limited to 1800 s to minimize the effects of cosmic rays, and the short exposures of 120 s or more were taken to measure the intensities of the brightest emission lines, which were close to saturation or saturated in longer exposures. The slit was east-west oriented and centered on the central star in each nebula. Table 2 lists the number and length of the exposures, the dispersion, the spectral resolution, measured as the full-width-at-half-maximum *FWHM* of the emission lines of comparison lamps, the wavelength range of the spectra, the telescope used and the date of the observations.

The data reduction (bias correction, flat-fielding, cosmic ray cleaning, wavelength and flux calibrations, 1D spectra extraction) was made using the *IRAF* software. In order to increase the signal-to-noise ratio, a rebinning of the CCD rows along the spatial direction was performed, giving a sampling of 1.64″ pxl^{-1}.

The line intensities were obtained by integrating the flux over a linear local continuum between two given limits. These measurements were made with the *splot* routine of the *IRAF* package. All the line intensities of a given spectrum were normalized to Hβ. The error associated with the line flux intensities were estimated by $\sigma^2 = \sigma^2_{\rm cont} + \sigma^2_{\rm line}$, where $\sigma_{\rm cont}$ and $\sigma_{\rm line}$ are the continuum rms and the Poisson error of the line respectively. The effect of the interstellar extinction was corrected by comparing the Hγ/Hβ and Hα/Hβ ratios measured in each aperture with the theoretical ones by Hummer (1987) for an electron temperature of 10 000 K and a density of 100 cm^{-3}. The Galactic reddening function of Savage & Mathis (1979) was used. The final intensity of a given emission line was the average of the line values corrected for interstellar extinction obtained from each spectrum.

The Balmer jump was measured by linearly fitting the observed continua on both sides of the discontinuity. On the blue side of the discontinuity, the continuum is well defined. However, on the red side the spectra were crowded by recombination lines and some extrapolation was required. The Balmer discontinuity, [$F_\lambda(\lambda3646-) - F_\lambda(\lambda3646+)$], was normalized to H$\beta$ using the observed intensity of H11. Due to the small separation between the Balmer discontinuity and the H11 line, the interstellar reddening is negligible. The errors in the Balmer discontinuity were obtained from the errors associated to the linear fittings of the continuum and from the error for the flux of H11.

3. Determination of the electron temperature and density

Electron temperatures were derived from the [O III](λ4959 + λ5007)/λ4363 and [N II](λ6548 + λ6583)/λ5755 intensity ratios and electron densities from the [S II]λ6716/λ6731, [Cl III]λ5517/λ5537, and [Ar IV]λ4711/λ4740 intensity ratios by solving numerically the equilibrium equations for a *n*-level atom using the *temden* routine of the *nebular* package of the *STSDAS/IRAF*. The references for the collision strengths C, transition probabilities T, and energy levels E used are listed in Table 3. For some planetary nebulae electron temperatures were also calculated from the ratio of the nebular Balmer discontinuity to Hβ, [$F_\lambda(\lambda3646-) - F_\lambda(\lambda3646+)$]/$F$(H$\beta$) by interpolation of the values presented by Osterbrock (1989).

There are several factors that can increase the errors in the measurement of electron density. The most significant factor is the saturation of line ratios at both low and high values of electron density. Stanghellini & Kaler (1989) consider that the measurements of electron density from [S II], [Cl III] and [Ar IV] ratios are reliable in the ranges $2.45 < \log N_{\rm e}({\rm cm}^{-3}) < 3.85$, $3 < \log N_{\rm e}({\rm cm}^{-3}) < 4.95$ and $3.3 < \log N_{\rm e}({\rm cm}^{-3}) < 5.55$, respectively. Other source of error for electron density determined from the [Ar IV]λ4740/λ4711 ratio is that the [Ar IV]λ4711 is blended with He Iλ4713. We discounted the helium contribution to this blend by assuming the intensity of the He Iλ4713 is one-tenth of the intensity of He Iλ4471 (Benjamin et al. 1999). The dependence of the electron density $N_{\rm e}$ on the assumed electron temperature $T_{\rm e}$ is another source of error. For the range of electron temperatures found in our sample of objects, the errors in the determinations of electron densities due to the assumption of a constant electron temperature in each nebula are below 5%, with exceptions of few density measurements with errors of the order of up to 20%.

In the determination of electron temperature there are many potential sources of uncertainty. For the electron temperatures

Table 1. Selected objects.

Object	α(2000)	δ(2000)	l	b	d(pc)	θ(″)	Other names
NGC 1535	$04^h14^m15^s.6$	$-12^h44^m22^s.5$	206°.48	−40°.56	1649 [2]	9.2 [2]	PK 206-40 1
					2140 [1]		
					2283 [3]		
NGC 2438	07 41 50.3	−14 44 08.8	231.80	4.12	1519 [2]	35.2 [2]	PK 231+04 2
					850 [1]		
					1203 [3]		
NGC 2440	07 41 55.3	−18 12 30.5	234.84	2.42	1088 [2]	16.4 [2]	PK 234+02 1
					1010 [1]		
					1348 [3]		
NGC 3132	10 07 01.7	−40 26 11.7	272.11	12.40	1079 [2]	28.0 [2]	PK 272+12 1
					1110 [1]		
					1251 [3]		
NGC 3242	10 24 46.0	−18 38 32.3	261.05	32.05	810 [2]	20.2 [2]	PK 261+321, Ghost of Jupiter Nebula
					860 [1]		
					1083 [3]		
NGC 6302	17 13 44.6	−37 06 11.7	349.51	1.06	415 [2]	22.3 [2]	PK 349+01 1, Bug Nebula, Gum 60
					950 [1]		
					525 [3]		
NGC 6563	18 12 02.5	−33 52 06.0	358.50	−7.34	1867 [2]	22.6 [2]	PK 358-07 1
					1270 [1]		
					1631 [3]		
NGC 6781	19 18 28.2	06 32 23.0	41.84	−2.99	904 [2]	35.0 [2]	PK 041-02 1
					910 [1]		
					699 [3]		
NGC 6853	19 59 36.2	22 43 15.6	60.84	−3.70	400 [2]	100.0 [2]	M 27, PK 060-03 1, Dumbbell Nebula
					250 [1]		
					262 [1]		
NGC 7009	21 04 10.8	−11 21 48.0	37.76	−34.57	871 [2]	13.4 [2]	PK 037-34 1, Saturn Nebula
					1280 [1]		
					1201 [3]		

References: [1] Cahn & Kaler (1971); [2] Maciel & Pottasch (1980); [3] Cahn et al. (1992).
Conventions: α, δ: equatorial coordinates; l, b: galactic coordinates, in degree; d: distance; θ: angular radius.
Catalogues: Gum = Gum (1955); PK = Perek & Kohoutek (1967).

estimated from the Balmer discontinuity the main difficulty lies in determining the continuum redward of the discontinuity, which is crowded by Balmer lines. Hence, the intensity of the continuum must be measured at longer wavelengths and extrapolated to λ3646+. For the electron temperatures measurements from the [O III](λ4959 + λ5007)/λ4363 and [N II](λ6548 + λ6583)/λ5755 ratios the greatest problem lies in the estimation of the flux of the [O III]λ4363 and [N II]λ5755 lines, which are very weak comparing with the other two lines of each ratio. However, this uncertainty is attenuated by the high signal-to-noise ratio of the data presented in this paper. An other source of error for electron temperature estimated from the [N II](λ6548 + λ6583)/λ5755 ratio is the contribution to the flux of the auroral line [N II]λ5755 due to recombination. The contribution reduces the electron temperature. For our sample of objects, it is only significant in the central regions of NGC 7009. We have estimated the recombination contribution to the intensity of the [N II]λ5755 line using the equation $I_R(\lambda 5755)/I(H\beta) = 3.19(T_e/10^4\,K)^{0.30} \times N^{++}/H^+$ given by Liu et al. (2000), assuming $N^{++}/H^+ = 3.10 \times 10^{-4}$ (Liu et al. 1995) for the central aperture and scaling this value by the flux in N IIλ5676 for other apertures. For the range of variation of the electron density found in the planetary nebulae studied the dependence of the electron temperature estimate on the assume electron density is practically insignificant, with exception of NGC 6302, in which high densities of the order of 15 000 cm^{-3} have been derived for the central region. The procedure to derive temperatures and densities from forbidden line ratios was as follows. We calculated the electron densities N_e(S II), N_e(Cl III), and N_e(Ar IV) assuming an initial electron temperature of 10 000 K. Then, a mean density for each nebula was used to derive the electron temperatures T_e(O III) and T_e(N II). Finally the electron densities were recalculated adopting mean values of electron temperature for each nebula. For NGC 6302, the T_e(N II) estimates are sensitive to the assume densities in the central region of nebula. Therefore, for this object different value of electron density were adopted for different apertures.

4. Results

Figures 1 and 2 present a sample of spectra from areas with different surface brightness showing the [N II]λ4363 and

Table 2. Journal of observations.

Object	Date	Telescope	$\Delta\lambda$ (Å)	*FWHM* (Å)	Disp. (Å pxl^{-1})	Exp. time (s)
NGC 1535	12.30.2002	1.52 m ESO	4630–6940	3.0	1.0	$3 \times 1200 + 4 \times 300$
	12.31.2002	1.52 m ESO	3120–5430	3.0	1.0	$3 \times 1200 + 3 \times 120$
NGC 2438	01.04.2002	1.52 m ESO	3840–5100	1.5	0.50	4×1500
	01.05.2002	1.52 m ESO	3840–5100	1.5	0.50	4×600
	05.02.2002	1.60 m LNA	6120–6900	2.8	0.75	3×1200
	12.30.2002	1.52 m ESO	4630-6940	3.0	1.0	3×1200
	12.31.2002	1.52 m ESO	3120–5430	3.0	1.0	3×1200
NGC 2440	01.05.2002	1.52 m ESO	3840–5100	1.5	0.50	$4 \times 1500 + 4 \times 120$
	05.02.2002	1.60 m LNA	6120–6900	2.8	0.75	4×600
	12.29.2002	1.52 m ESO	3120-5430	3.0	1.0	$3 \times 1500 + 6 \times 120$
	12.30.2002	1.52 m ESO	4630–6940	3.0	1.0	$2 \times 600 + 6 \times 100$
NGC 3132	12.31.2002	1.52 m ESO	3120–5430	3.0	1.0	3×600
	12.31.2002	1.52 m ESO	4630–6940	3.0	1.0	$1 \times 1200 + 1 \times 100$
NGC 3242	05.02.2002	1.60 m LNA	6120–6900	2.8	0.75	$1 \times 300 + 2 \times 1200$
	01.04.2002	1.52 m ESO	3840–5100	1.5	0.50	$2 \times 600 + 3 \times 120$
	01.05.2002	1.52 m ESO	3840-5100	1.5	0.50	3×600
	07.10.2002	1.52 m ESO	3300–5100	3.0	0.75	4×1200
	07.10.2002	1.52 m ESO	4460-6800	3.0	0.75	3×600
	07.09.2002	1.52 m ESO	4490-6860	3.0	0.75	$6 \times 300 + 1 \times 120$
NGC 6302	07.09.2002	1.52 m ESO	4490–6860	3.0	0.75	$4 \times 1800 + 4 \times 150$
	07.10.2002	1.52 m ESO	3300–5100	3.0	0.75	3×600
NGC 6563	07.10.2002	1.52 m ESO	4460–6800	3.0	0.75	3×1200
NGC 6781	07.09.2002	1.52 m ESO	4690–6860	3.0	0.75	2×1200
NGC 6853	07.09.2002	1.52 m ESO	4490–6860	3.0	0.75	3×1200
	07.10.2002	1.52 m ESO	4460–6800	3.0	0.75	2×1200
NGC 7009	09.12.1994	1.60 m LNA	4100–5030	2.8	1.0	$9 \times 120 + 8 \times 600$
	09.12.1994	1.60 m LNA	6200–7000	2.8	1.0	$9 \times 120 + 2 \times 600$
	07.09.2002	1.52 m ESO	4490-6860	3.0	0.75	15×120
	07.10.2002	1.52 m ESO	4460-6800	3.0	0.75	$2 \times 1200 + 2 \times 600$
	07.10.2002	1.52 m ESO	3300-5100	3.0	0.75	3×1200

Table 3. Line ratios and references for the atomic data.

Line ratios	T	C	E
[O III](λ 4959 + λ 5007)/λ 4363	[6]	[2]	[1,8]
[N II](λ 6548 + λ 6583)/λ 5755	[6]	[2]	[1,9]
[S II]λ 6716/λ 6731	[7,10]	[3]	[1,10]
[Cl III]λ 5517/λ 5537	[11,12]	[4]	[1]
[Ar IV]λ 4711/λ 4740	[12,13]	[5]	[1]

References: [1] Bowen (1960); [2] Lennon & Burke (1994); [3] Ramsbottom et al. (1996); [4] Butler & Zeippen (1989); [5] Zeippen et al. (1987), [6] Wiese et al. (1996); [7] Keenan et al. (1993); [8] Moore (1985); [9] Williams & Livio (1995); [10] Verner et al. (1996); [11] Mendoza (1983); [12] Kaufman & Sugar (1986); [13] Mendoza & Zeippen (1982).

[N II]λ 5755 lines for NGC 6302 and NGC 2440. Figure 3 shows the Balmer discontinuity and our fitting of the observed continua for NGC 7009. Spatial profiles along the slit of the Hβ flux, electron temperature and electron density are shown in Figs. 6–23. Table 4 presents some statistics of the electron temperature and density measurements, including the number N of distinct nebular areas, the median, the first and the third quartiles, *Q1* and *Q3* respectively (limits between which 50% of the values lie), the minimum and maximum, and the mean and the standard deviation σ weighted by the flux in Hβ. Next, the observed objects are discussed separately.

4.1. NGC 1535

NGC 1535 is a bright planetary nebula with a pronounced ring structure of about $20'' \times 17''$ within a fainter, larger disk of about $48'' \times 42''$ (Perek & Kohoutek 1967). This object shows a rich spectrum of rather high excitation. The intensities of emission lines of low ionization species such as those of [S II], [Cl III], and [N II] were not measurable in our spectra. The electron densities were estimated only by the [Ar IV]λ 4711/λ 4740 ratio, a density indicator for more internal zones of nebulae. A mean value of N_e(Ar IV) = 2049 ± 166 cm^{-3} was estimated, which is consistent with measurements by other authors (Minkowski & Aller 1956; Aller & Walker 1965; Gutierrez-Moreno et al. 1985). The data obtained for NGC 1535 (Figs. 4 and 5) show low amplitude variations of electron density and temperature with the position along the radius of the nebula. We have found that T_e(O III) are systematically higher than T_e(Bal), with mean values of T_e(O III) = 12 607 ± 148 K and T_e(Bal) = 10 131 ± 105 K. This discrepancy between T_e(O III) and T_e(Bal) was also found by other authors

Table 4. Electron temperature and density statistics.

	N	min	*Q1*	median	*Q3*	max	mean	σ
NGC 1535								
N_e(Ar IV) (cm^{-3})	24	580	1425	1671	2430	3722	2049	813
T_e(O III) (K)	29	11 672	12 018	12 349	12 709	15 489	12 607	799
T_e(Bal) (K)	9	9810	9743	9923	10 371	10 560	10 131	315
NGC 2438								
N_e(S II) (cm^{-3})	49	19	98	155	209	340	158	64
T_e(N II) (K)	32	10 265	10 843	11 173	11 461	12 265	11 245	490
T_e(O III) (K)	45	10 662	11 026	11 590	12 373	14 080	11 541	840
NGC 2440								
N_e(S II) (cm^{-3})	35	256	458	806	1891	3360	2551	1670
N_e(Cl III) (cm^{-3})	14	487	2426	3131	5276	5477	4131	1809
N_e(Ar IV) (cm^{-3})	25	0	1032	1572	3031	4186	3192	1694
T_e(N II) (K)	35	9493	10 692	11 822	12 491	14 086	11 838	1152
T_e(O III) (K)	43	13 084	13 612	13 623	14 673	19 291	14 398	1302
T_e(Bal) (K)	12	11 178	11 929	14 323	14 993	18 886	13 984	2218
NGC 3132								
N_e(S II) (cm^{-3})	37	110	335	558	714	910	617	239
N_e(Cl III) (cm^{-3})	15	953	1372	1870	2891	4980	2045	1138
N_e(Ar IV) (cm^{-3})	15	399	1266	1867	2333	5751	2278	1533
T_e(N II) (K)	30	9577	9987	10357	10 749	12 456	10 163	726
T_e(O III) (K)	24	9411	9413	9682	10 325	12421	9889	721
NGC 3242								
N_e(S II) (cm^{-3})	13	1150	2332	2818	3845	7643	3 081	1 640
N_e(Cl III) (cm^{-3})	19	201	1381	1822	3183	11 602	3 188	2 757
N_e(Ar IV) (cm^{-3})	29	576	1851	2629	3525	4413	3247	1156
T_e(O III) (K)	35	11 201	11 565	12 252	12 881	16 792	12 213	1 378
T_e(Bal) (K)	24	8055	8907	9692	9864	10 150	9541	652
NGC 6302								
N_e(S II) (cm^{-3})	91	11	238	797	1669	14 509	6 811	5 846
N_e(Cl III) (cm^{-3})	43	362	2977	7468	15 890	130 192	37 694	34 280
N_e(Ar IV) (cm^{-3})	51	88	2283	4 590	8 121	15 939	10 238	6 178
T_e(N II) (K)	94	11 437	12 001	12 428	13 016	17 771	13 798	1580
T_e(O III) (K)	80	15 009	16 443	17 071	17 889	20 461	18 357	1596
NGC 6563								
N_e(S II) (cm^{-3})	47	1	70	142	176	267	134	70
T_e(N II) (K)	43	9835	10 522	10 731	11 059	12 421	10 743	471
NGC 6781								
N_e(S II) (cm^{-3})	57	1	40	131	233	343	135	94
T_e(N II) (K)	31	9208	10 391	10 913	11 386	12 927	10 763	781
NGC 6853								
N_e(S II) (cm^{-3})	126	4	40	88	131	553	95	80
T_e(N II) (K)	142	9488	10 450	10 832	11 146	12 629	10 898	572
NGC 7009								
N_e(S II) (cm^{-3})	35	253	806	2352	3152	3598	3164	1683
N_e(Cl III) (cm^{-3})	19	1793	4980	5363	7294	7909	6239	1610
N_e(Ar IV) (cm^{-3})	13	471	891	2735	7448	9930	4314	3143
T_e(N II) (K)	17	9847	10 477	10 749	11 524	12 487	11 163	785
T_e(O III) (K)	27	8534	9503	9856	10 184	11 740	10 117	761
T_e(Bal) (K)	21	7340	8250	8521	8740	9045	8589	500

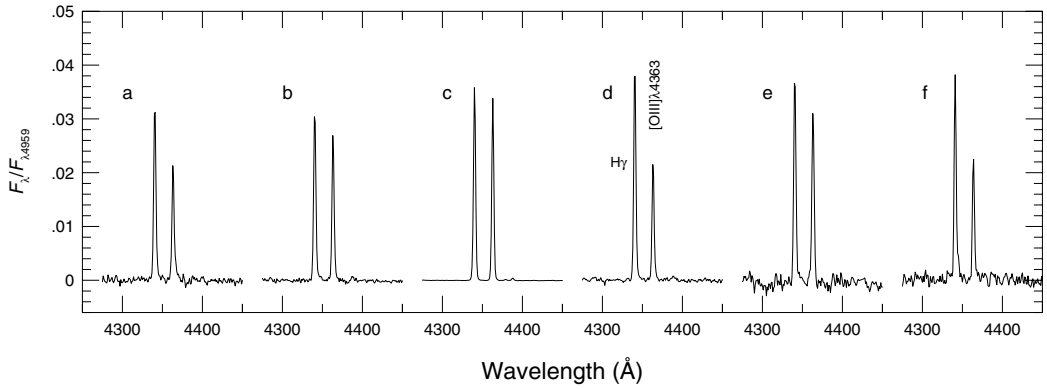

Fig. 1. A sample of spectra in the range of 4275 to 4460 Å from areas with different surface brightnesses for NGC 6302. The corresponding positions are marked in Fig. 15. To emphasize the variation of the [O III](λ 4959 + λ 5007)/λ 4363 ratio, the flux scale was normalized to the peak of [O III]λ 4959.

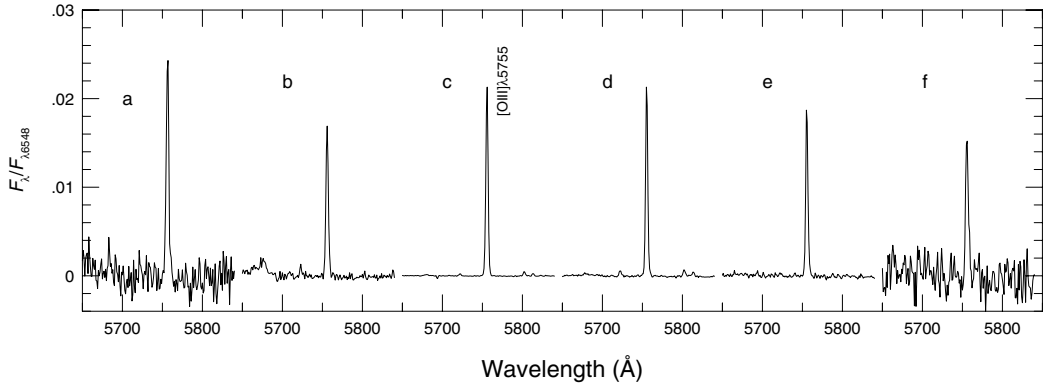

Fig. 2. A sample of spectra in the range of 5650 to 5850 Å from areas with different surface brightnesses for NGC 2440. The corresponding positions are marked in Fig. 9. To emphasize the variation of the [N II](λ 6548 + λ 6583)/λ 5755 ratio, the flux scale was normalized to the peak of [N II]λ 6548.

in other planetary nebulae and was attributed to temperature fluctuations ranging on average from $t^2 = 0.03$ to $t^2 = 0.07$ (Peimbert 1971; Liu & Danziger 1993; Zhang et al. 2004).

4.2. NGC 2438

This planetary nebula exhibits a bright, round inner ring and a detached faint halo. Figure 6 shows a very smooth variation of density with a weighted mean value of N_e(S II) = 158 ± 9 cm^{-3}. The low electron densities found in NGC 2438 are characteristic of objects in a more advanced stage of nebular evolution. This interpretation was given by Guerrero & Manchado (1999) and is in agreement with the dynamical age of around 17 000 yr derived from an expansion velocity of 22 km s^{-1} (Meatheringham et al. 1988) and a distance of 2.0 kpc (Pottasch 1983).

The electron temperatures estimated from the [O III](λ 4959 + λ 5007)/λ 4363 and [N II](λ 6548 + λ 6584)/λ 5755 ratios (see Fig. 7) present variations of small amplitude along the slit. The mean electron temperatures derived from these two line intensity ratios are in good agreement. We found weighted mean electron temperatures of T_e(O III) = 11 541 ± 125 K and T_e(N II) = 11 245 ± 87 K.

The spatial variation of the temperature T_e(O III) has a behavior opposite to the profile of the surface nebular brightness, with the surface brightness in Hβ decreasing with the increase of electron temperature. This was also found in 30 Doradus (Krabbe & Copetti 2002). A possible interpretation of such behavior is that it might be indicating an anti-correlation between [O III] temperature and density. In fact, such anti-correlation, although somewhat subtle, can be seen in our data for NGC 2438, with the density increasing and electron temperature decreasing in the direction of the areas with higher surface brightness.

4.3. NGC 2440

NGC 2440 is a bipolar planetary nebula that may be taken as the prototype of Peimbert type I (Peimbert 1978), an object rich in He and N. It is a bright, somewhat elongated object which shows two distinct central condensations with fainter outer filaments and it has a wide variety of surface brightness and excitation. The density profiles obtained for NGC 2440 from the [S II], [Ar IV], and [Cl III] ratios (see Fig. 8) show a well defined spatial gradient, with the density decreasing from the center to the edges. The densities derived from these three ratios show similar variations across the nebular surface. We have

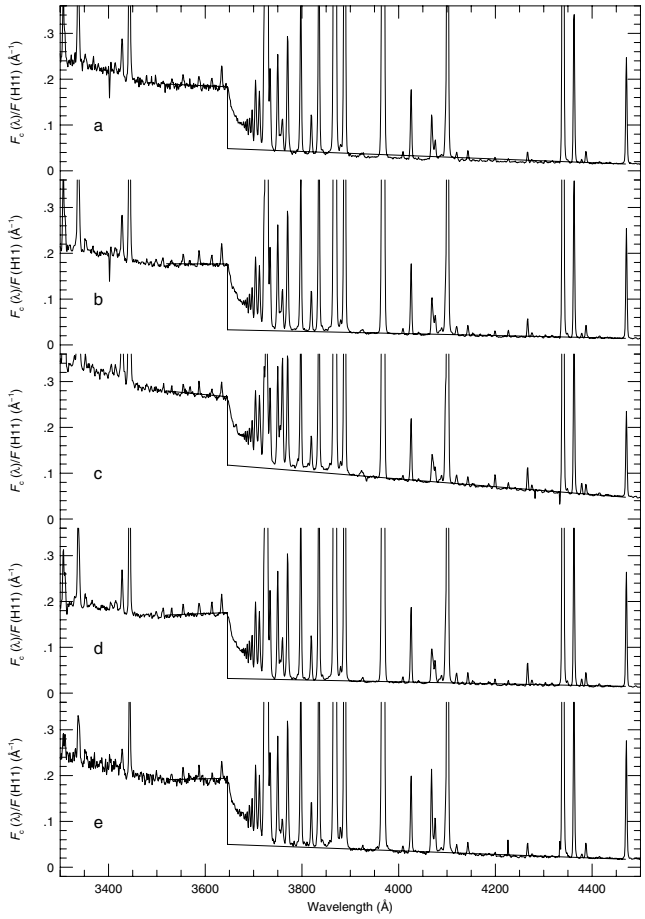

Fig. 3. A sample of spectra showing the observed Balmer discontinuity from different surface brightnesses for NGC 7009. The corresponding positions are marked in Fig 9. The scale of flux was normalized to the flux of H11.

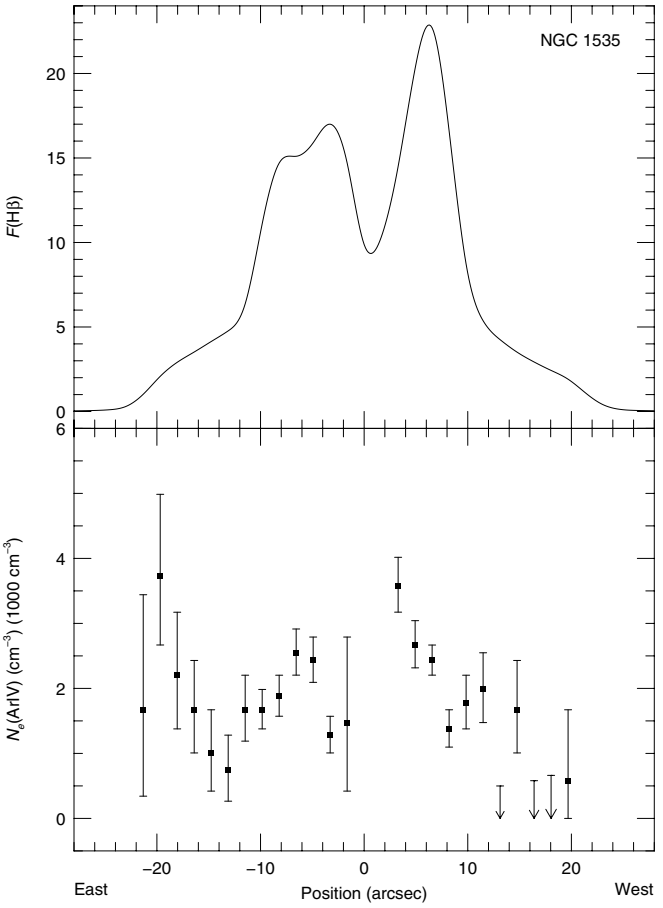

Fig. 4. NGC 1535. Spatial profiles of Hβ flux (in units of 10^{-14} erg cm^{-2} s^{-1}) and N_e(Ar IV).

derived mean electron densities of N_e(S II) = 2 551 ± 282 cm^{-3}, N_e(Cl III) = 4 131 ± 483 cm^{-3}, and N_e(Ar IV) = 3 192 ± 339 cm^{-3}. Our mean electron densities are systematically lower than the ones derived by Shields et al. (1981). We have recalculated the electron densities from their [S II], [Ar IV], and [Cl III] ratios using the same atomic parameters and electron density adopted in this paper, and we have derived values from about 1000 to 2000 cm^{-3} higher than those from our own data. However, these authors have concentrated their observations on the nebular core, where the values of electron density are systematically higher.

As can be seen in the Fig. 9, the electron temperatures derived from the [O III] and [N II] ratios and from the observed Balmer discontinuity show a systematic variation across the nebular surface. The electron temperatures derived from the [N II] and [O III] ratio are decreasing from the centre to the edges in the area of the nebula with higher surface brightness in Hβ and increasing in the direction of the outskirts of the nebula, where the surface brightness is lower. At the same time, the profile of Balmer temperature is completely different of the profiles of [N II] and [O III] temperatures, not showing any relation with the surface brightness of the nebula. For the entire set of apertures observed we found weighted mean electron temperatures of T_e(O III) = 14 398 ± 199 K, T_e(N II) = 11 838 ± 195 K, and T_e(Bal) = 13 984 ± 640 K. The [O III] temperatures are in good agreement with those obtained by Hyung & Aller (1998), Liu & Danziger (1993), Peimbert & Torres-Peimbert (1987), Gutierrez-Moreno et al. (1985) and Shields et al. (1981); however the mean electron temperature derived for the [N II] zone by these authors are about 1000 to 2000 K lower than the ones obtained from our own observations. On the other hand, our estimations are compatible with the ones of T_e(N II) = 11 500 K and T_e(N II) = 13 800 K found in two regions of NGC 2440 by Boeshaar (1974). If these higher temperatures are an artifact of the line flux estimation it will be certainly due to the errors in the intensities of the [N II]λ 5755 line, since weak emission lines are biased towards overestimated values (Rola & Pelat 1994). However, our intensities of [N II]λ 5755 line have high signal-to-noise ratio and therefore the errors associated with these measurements are not considerable.

Higher electron temperatures have been estimated from other indicators. Rowlands et al. (1989) derived electron temperatures of 17 100 K using the [Ne V](λ 24.3 μm/λ 3426 Å) ratio and 22 000 K using the [O IV](λ 25.9 μm/λ 1400 Å) ratio. Although the temperature estimates derived from [Ne V](λ 24.3 μm/λ 3426 Å) are quite dependent on electron

density and hence more susceptible to uncertainties, these high temperatures are an indication of the presence of considerably hotter zones in the inner part of the nebula.

4.4. NGC 3132

This is a moderately high excitation planetary nebula showing an elliptical structure. As for NGC 2440, the nitrogen is enhanced in the ionized material and it can be placed in the Peimbert type I category (Peimbert 1978). The results for this object are illustrated in Figs. 10 and 11. Due to the presence of a bright central star some emission lines from the central region of the nebula were more susceptible to uncertainties or could not be measured. A well defined spatial variation of the [S II] density has been observed in this object with two density peaks of $N_e(\mathrm{S\,II}) = 910^{+38}_{-35}$ cm^{-3} and $N_e(\mathrm{S\,II}) = 874^{+36}_{-34}$ cm^{-3} along the east-west direction. The position of the density peak on the east side is shifted for about 3″ to the east of the Hβ peak and the density peak on the west side is about 1″ away from the Hβ peak on the west. The [S II] densities seem to have a similar density variation of NGC 2438, that is, the electron density is increasing with the increase of surface brightness in Hβ, although this is not so clear in the central part, where the measurements are more doubtful. Juguet et al. (1988) have determined densities from the [S II]λ 6716/λ 6731 ratio and they have found a double peaked distribution along the north-south direction, reaching up to $N_e(\mathrm{S\,II}) = 1300$ cm^{-3} at the outer region and decreasing to $N_e(\mathrm{S\,II}) = 300$ cm^{-3} at the central position. Unfortunately, for the [Ar IV] and [Cl III] densities it is not possible to observe a variation similar to that of the [S II] densities, probably because there are few measurements of [Ar IV] and [Cl III] densities along the nebular surface. We have derived mean densities of $N_e(\mathrm{Cl\,III}) = 2045 \pm 304$ cm^{-3} and $N_e(\mathrm{Ar\,IV}) = 2\,278 \pm 425$ cm^{-3}, which are about 1500 cm^{-3} higher than the [S II] mean density.

The profiles of [N II] and [O III] temperatures shows smooth variations across the nebula. Although it was not possible to estimate the electron temperatures in the central region of nebula, the [N II] and [O III] temperatures seem to present profiles similar to that of the [O III] temperature in NGC 2438 and the same anti-correlation between temperature and surface nebular brightness. The derived mean temperatures of $T_e(\mathrm{N\,II}) = 10\,163 \pm 133$ K and $T_e(\mathrm{O\,III}) = 9\,889 \pm 147$ K are compatible with the estimates of Torres-Peimbert & Peimbert (1977) and Baessgen & Grewing (1990).

4.5. NGC 3242

NGC 3242 is a high excitation nebula showing a bipolar structure in the central region with a fainter outer halo. Figures 12 and 13 show the results obtained for this nebula. The densities obtained from the [S II]λ 6716/λ 6731 and [Cl III]λ 5517/λ 5537 intensity ratios are relatively homogeneous, with mean values of $N_e(\mathrm{S\,II}) = 3\,081 \pm 455$ cm^{-3} and $N_e(\mathrm{Cl\,III}) = 3\,188 \pm 632$ cm^{-3}. However, the uniformity of the density distribution may be apparent to the fact that the [Cl III] and [S II] lines are somewhat faint, so the derived density values are rather uncertain. Densities derived from the [Ar IV]λ 4711/λ 4740 ratio present a smooth variation increasing as the surface brightness Hβ increases. The densities inferred from [Cl III], [S II], and [Ar IV] emission lines are compatible, indicating that the density is not correlated with the ionization state.

The distribution of electron temperatures estimated from the [O III] ratio and from the observed Balmer discontinuity exhibits variations of very low amplitude across the nebula. Fig. 13 shows that the temperatures obtained from [O III] ratio are systematically higher than those inferred from the observed Balmer discontinuity. We have found mean temperatures of $T_e(\mathrm{O\,III}) = 12\,213 \pm 233$ K and $T_e(\mathrm{Bal}) = 9\,541 \pm 133$ K, which agree well with the values measured by Liu & Danziger (1993). Again, the [O III] temperature tends to increase as the surface brightness in Hβ increases at the brightest parts of the nebula. Higher temperatures are also found at the outskirts of the nebula.

4.6. NGC 6302

This planetary nebula is one of the brightest known in our galaxy. Indeed it is the object in our sample with the highest surface brightness. The optical image of NGC 6302 shows an impressive bipolar morphology. Such nebula has been classified as type I in the scheme of Peimbert & Torres-Peimbert (1983), with abundances even more extreme than typical type I nebulae (Aller et al. 1981). Figure 14 reveals a systematic variation with the position in the nebula of the electron densities obtained from the [S II]λ 6716/λ 6731, [Ar IV]λ 4711/λ 4740, and [Cl III]λ 5517/λ 5537 ratios. The densities derived from these three ratios show similar spatial variations, peaking at the centre of the nebula and decreasing from the centre to the outer regions. This object has the highest electron densities in our sample, with a mean density of $N_e(\mathrm{S\,II}) = 6\,811 \pm 613$ cm^{-3}, $N_e(\mathrm{Cl\,III}) = 37\,694 \pm 5\,228$ cm^{-3}, and $N_e(\mathrm{Ar\,IV}) = 10\,238 \pm 865$ cm^{-3}. In particular, the [Cl III] densities are higher than the [S II] and [Ar IV] densities.

The [O III] and [N II] electron temperatures (see Fig. 15) also show well defined systematic variation along the nebular surface, with peak values of $T_e(\mathrm{O\,III}) = 19\,865^{+55}_{-54}$ K and $T_e(\mathrm{N\,II}) = 15\,407^{+125}_{-127}$ K in the central region of the nebula. The profiles of [O III] and [N II] electron temperatures are similar to each other, with the electron temperature increasing in the direction of the areas with higher surface brightness in Hβ. Again, at the outskirts of the nebula higher temperatures are found. This nebula has also the highest electron temperatures in our sample, with mean values of $T_e(\mathrm{O\,III}) = 18\,357 \pm 178$ K and $T_e(\mathrm{N\,II}) = 13\,798 \pm 163$ K.

4.7. NGC 6563

NGC 6563 is an object that appears on Hα images (Chu et al. 1987) as a fairly elliptical planetary nebula with brightening at the ends of the minor axis. Our observations have revealed that the electron temperature and density are relatively homogeneous (see Figs. 16 and 17) with mean values of

T_e(N II) = 10 743 ± 72 K and N_e(S II) = 134 ± 10 cm^{-3}. The low densities found here are evidence of a relatively evolved object. At the distance of 1 867 kpc (Maciel & Pottasch 1980) and with an angular radius of 22.6″ (Perek & Kohoutek 1967), the expansion velocity of 11 km s^{-1} measured by Weinberger (1989) yields a dynamical age of 17.8×10^3 yr for NGC 6563.

4.8. NGC 6781

This is a planetary nebula with low surface brightness. Mavromatakis et al. (2001) mapped this nebula in several optical emission lines and these images display a known "C" like structure. The electron densities (see Fig. 18) are relatively low with a mean value of N_e(S II) = 135 ± 12 cm^{-3}. Since the [S II]λ6716/λ6731 ratios are close to the low density limit the density measurements are more susceptible to errors; therefore the mean value derived of N_e(S II) = 214 cm^{-3} by Liu et al. (2004) seems relatively compatible with our mean estimate. An age of 40 000 yr was determined by Mavromatakis et al. (2001) indicating that it is an evolved object. The electron temperatures distribution derived from the [N II] ratio is relatively uniform, with a mean of T_e(N II) = 10 763 ± 140 K, which is consistent with the findings by Mavromatakis et al. (2001) and Liu et al. (2004).

4.9. NGC 6853

The nebula NGC 6853, also known as Dumbbell Nebula, has a wide range of ionization as showed by Hawley & Miller (1978). It is the nebula with the largest angular size in our sample. This object has a low surface brightness and irregular shape. NGC 6853 presents a relatively homogeneous electron density distribution (see Fig. 20), with a mean density of N_e(S II) = 95 ± 7 cm^{-3}. This is the object with the lowest density in our sample. The low densities in this nebula indicate that it is a relatively evolved object. The distribution of electron temperature (see Fig. 21) is about constant along the nebular surface. For the entire set of 142 apertures observed, we found a weighted mean electron temperature of T_e(N II) = 10 898 ± 48 K. Barker (1984) has measured the electron density and temperature in seven different positions for NGC 6853 finding a mean temperature of T_e(N II) = 10 529 K, in accordance with our measurements.

4.10. NGC 7009

NGC 7009, sometimes called the Saturn Nebula, is a high surface brightness planetary nebula which has been well studied both observationally and theoretically. This nebula shows an elliptical structure with striking ansae (Aller 1941), that is, pairs of low ionization knots. Figure 22 shows the spatial variation of the electron density derived from the [S II], [Cl III], and [Ar IV] ratios. The electron density derived from these three ratios presents a well defined variation of the density with the position along the nebular surface, with the density increasing in the direction of the higher surface brightness. We have estimated weighted mean electron densities of N_e(S II) = 3 164 ± 284 cm^{-3}, N_e(Cl III) = 6 239 ± 369 cm^{-3}, and N_e(Ar IV) = 4 314 ± 872 cm^{-3}.

The electron temperature estimates obtained from the [N II] and [O III] ratios and Balmer discontinuity (see Fig. 23) show systematic variation along the direction observed, with the temperature increasing with the increase of the surface brightness. We have derived mean temperatures of T_e(N II) = 11 163 ± 196 K, T_e(O III) = 10 117±146 K, and T_e(Bal) = 8 589±109 K. If we neglect the recombination excitation contribution to the [N II]λ5755 line, the [N II] temperatures would be overestimated, particularly in the central parts of NGC 7009, and consequently we would obtain a spurious spatial gradient of [N II] temperature. Neglecting the correction for the recombination contribution to the [N II]λ5755 line, we would derive a mean temperature of T_e(N II) = 13 681 ± 732 K, which is about 2500 K higher than corrected value.

Many papers have been published about the physical properties of NGC 7009 (Gonçalves et al. 2003; Rubin et al. 2002; Liu et al. 1995; Barker 1983; Czyzak & Aller 1979), and in general our estimates are compatible with previous determinations of temperatures and densities. Rubin et al. (2002) have evaluated the [O III] electron temperature variation along the major axis of NGC 7009, with spectrophotometric data obtained with the Hubble Space Telescope at a spatial resolution of 0.05 arcsec. Interestingly, they have also found a similar behaviour of temperature across the nebula. Gonçalves et al. (2003) have also presented estimates of temperature and density for eight different regions, along the major axis of NGC 7009. They have found the [O III] and [N II] electron temperatures remarkably constant throughout the nebula, with a average value of T_e(O III) = 10 200 K and T_e(N II) = 11 100 K.

5. Discussion

5.1. Comparison of electron densities

For five planetary nebulae in our sample, namely NGC 2440, NGC 3132, NGC 3242, NGC 6302, and NGC 7009, it was possible to compare the electron densities derived from the [S II](λ6716/λ6731), [Cl III](λ5517/λ5537), and [Ar IV](λ4711/λ4740) ratio lines. It is important to realize that the [S II] ratio is a density sensor for the outer parts of the nebula, while the [Cl III] and [Ar IV] ratios are density indicators for the intermediate and inner parts of the nebula, respectively. From our estimates we have found that in general N_e(Cl III) > N_e(Ar IV) > N_e(S II) for NGC 2440, NGC 6302, and NGC 7009. As discussed by Stanghellini & Kaler (1989), N_e(Cl III) > N_e(Ar IV) indicates that the [Ar IV] lines are produced in a rarefied inner region. For NGC 3132 and NGC 3242, the mean densities derived from the [Cl III] and [Ar IV] ratios are approximately similar to each other; at the same time the densities determined from the [S II] ratio are substantially lower. These differences can occur because the S^+ zone is basically separated of both Ar^{+3} and Cl^{+2} zones.

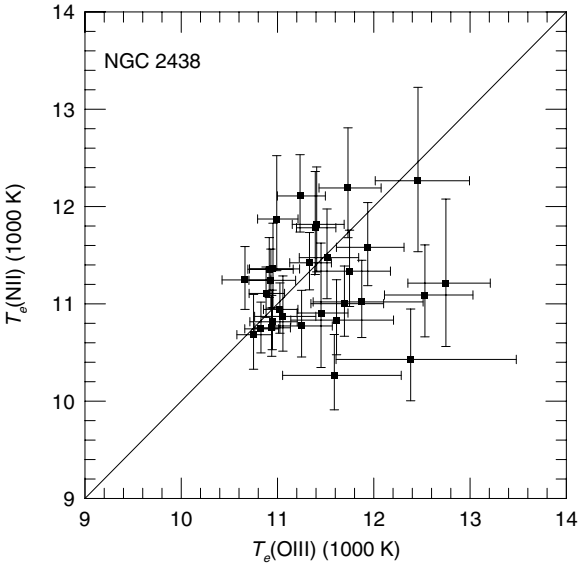

Fig. 24. T_e(N II) vs. T_e(O III) for NGC 2438.

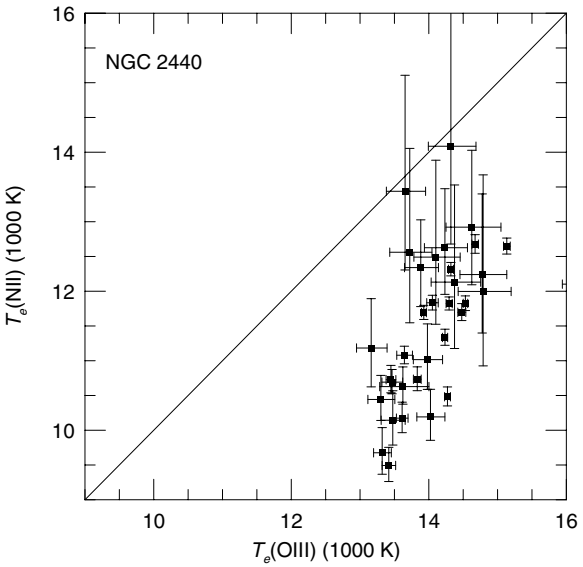

Fig. 25. Same as Fig. 24, but for NGC 2440.

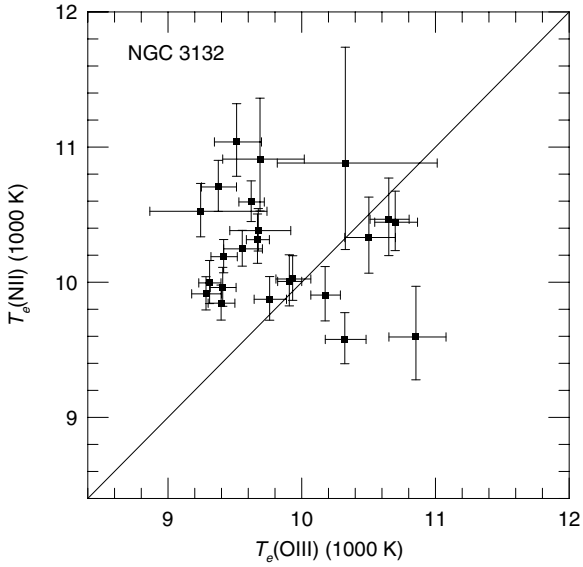

Fig. 26. Same as Fig. 24, but for NGC 3132.

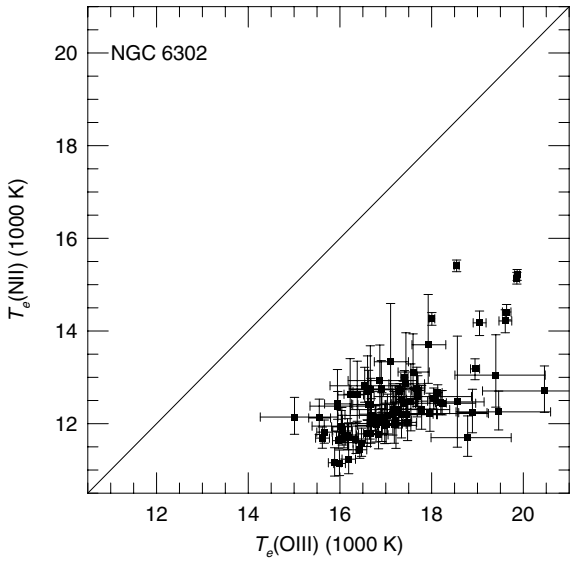

Fig. 27. Same as Fig. 24, but for NGC 6302.

5.2. Comparison of electron temperatures

Electron temperatures derived from different indicators can present considerable differences. These differences can be caused by temperature variations inside a given nebula. Kaler (1986) has showed that the mean ratio of T_e(N II)/T_e(O III) varies as a function of overall nebular excitation. He found that as central star temperature increases from $T_* \sim 25\,000$ K to ~50 000 K, this ratio increases from ~0.7 to ~1.1, and then decreases to 0.7 again for the highest levels of excitation. In Figs. 24–28 we have plotted T_e(N II) versus T_e(O III) for NGC 2438, NGC 2440, NGC 3132, NGC 6302, and NGC 7009.

We have found that T_e(N II) < T_e(O III) in NGC 2440 and NGC 6302, which are high excitation objects. For NGC 2438 and NGC 3132, which are low excitation objects, we verified that T_e(N II) ≈ T_e(O III). In the case of NGC 7009, T_e(N II) > T_e(O III), with exception of two points.

Figures 5, 9, 13 and 23 show that T_e(O III) is systematically higher than T_e(Bal), although there are a few exceptions. On average, T_e(O III) is about 20% higher than T_e(Bal). As the nebular continuum emission is due to a recombination process, the T_e(Bal) values are weighted towards lower temperature regions, whereas the fluxes of collisionally excited lines are preferentially weighted towards higher temperature regions, so these higher [O III] temperatures are expected.

5.3. Electron temperature versus density

We found two different kinds of relationship between electron temperature and surface brightness or electron density. For NGC 2440, NGC 6302, and NGC 7009 we have found a correlation between electron temperature and electron density or surface brightness, with the electron temperature increasing with the increase of the electron density or surface brightness.

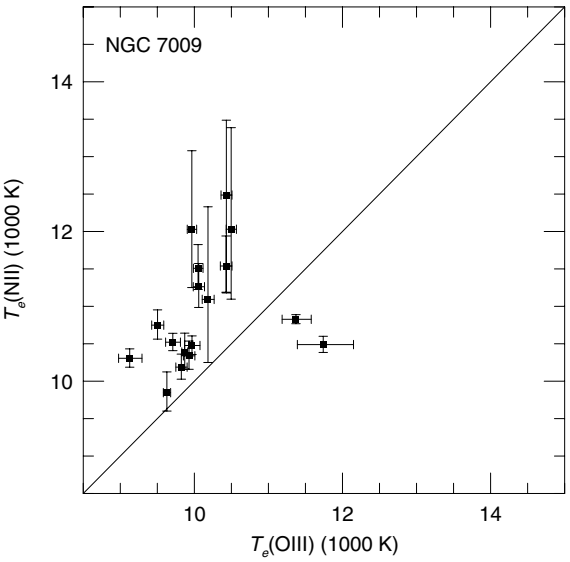

Fig. 28. Same as Fig. 24, but for NGC 7009.

For NGC 3242 and NGC 1535 we have also found a correlation between [O III] electron temperature and [Ar IV] electron density, although this correspondence is rather subtle. On the other hand, we have found an opposite relation between electron temperature and electron density for NGC 2438 and NGC 3132, with the [O III] electron temperature increasing with the decrease of the [S II] electron density, although this fact is not so clear for NGC 2438 because the [S II] ratios are close to the low density limit and this behaviour is somewhat masked. For the remaining objects NGC 6563, NGC 6781, and NGC 6853 it was not possible to detect any relationship between electron temperature and surface brightness. These objects present irregular surface brightness and the electron temperature and density profiles are fairly homogeneous. Figure 29 plots the T_e(O III) versus N_e(S II) for NGC 2440 and NGC 6302.

The correlation and anti-correlation between temperature and density found in our sample of objects seem to be associated with the structure of the nebula. NGC 2438 and NGC 3132, in which we have found the anti-correlation between temperature and density, are classical example of ring shaped nebulae. So, as a cavity is present in the central region of these nebulae higher densities are expected in the bright ring and lower densities in the central region of the nebula. An anti-correlation between [O III] temperature and density has also been found for the planetary nebula NGC 6720 (Garnett & Dinerstein 2001; Guerrero et al. 1997), which is also a ring shaped nebula. On the other hand, NGC 2440, NGC 3242, NGC 6302, and NGC 7009, in which a correlation between temperature and density is present, are bipolar planetary nebulae that are denser in the central regions.

In most of objects (NGC 1535, NGC 2438, NGC 2440, NGC 3132, NGC 3242, and NGC 6302) we have found high temperatures at the outskirts of the nebula, where low surface brightnesses and densities are present. All these facts indicate that the density structure may play an important role in the production of temperature fluctuations.

5.4. Magnitude of the electron temperature fluctuations

In order to characterize temperature fluctuations and their effects on forbidden line abundance determination, Peimbert (1967) introduced the concepts of the mean ionic temperature T_0 and the temperature fluctuation parameter t^2, defined as

$$t^2 = \frac{\int (T_e - T_0)^2 N_i N_e dV}{T_0^2 \int N_i N_e dV}, \quad (1)$$

$$T_0 = \frac{\int T_0 N_i N_e dV}{\int N_i N_e dV}, \quad (2)$$

where N_i is the density of the ion used to measure the temperature and the integrations are calculated over the observed volume of the nebula.

The t^2 parameter cannot be measured directly, so estimations have been obtained by comparing the abundances derived from forbidden and recombination lines. The values of t^2 required to reconcile the differences in the measurements of abundances determined by these two methods are high and lie in a range of $0.02 \leq t^2 \leq 0.10$. For example, for the Orion Nebula, Esteban et al. (1999) estimated $t^2 \approx 0.024$, while for NGC 7009, Liu et al. (1995) found $t^2 \approx 0.1$.

A discrete estimation of t^2 can be obtained through point-to-point determinations of the electron temperature across the nebula, using the expression given by Liu (1998)

$$t_s^2 = \frac{\sum_i (T_e^i - T_0)^2 F_i(H\beta)}{T_0^2 \sum_i F_i(H\beta)}, \quad (3)$$

where T_e^i and $F_i(H\beta)$ are the electron temperature and the Hβ flux obtained for the aperture i respectively. Part of the observed relative variance t_s^2(obs) is due to errors in the measurements, so the final estimation of t_s^2 must be corrected by $t_s^2 = t_s^2(\text{obs}) - t_{er}^2$, being t_{er}^2 the relative mean quadratic error of the electron temperature measurements.

The measurements of temperature reported here correspond to mean values inside the apertures and along the line of sights, so any small-scale temperature fluctuation would be smoothed out by the present observations. For this reason, it is clear that t_s^2 can only give a lower limit to t^2. However, the determination of t_s^2 appears to be the only direct way to estimate t^2.

In Table 5 the values of t_s^2 for the distributions of temperatures T_e(O III), T_e(N II), and T_e(Bal) are presented. We have estimated values of t_s^2(Bal) ranging from 0.0003 to 0.0078, t_s^2(N II) from 0.0003 to 0.0097, and t_s^2(O III) from 0.0011 to 0.0050.

Until now, low values of temperature fluctuations have also been found from point-to-point measurements of electron temperature for other objects: t_s^2(O III) = 0.002 for the planetary nebula NGC 4361 (Liu 1998), t_s^2(O III) = 0.0035 for the planetary nebula NGC 7009 (Rubin et al. 2002), t_s^2(O III) = 0.0025 for the 30 Doradus Nebula (Krabbe & Copetti 2002), and t_s^2(O III) = 0.00682–0.0176 and t_s^2(N II) = 0.00584–0.0175 for Orion Nebula (Rubin et al. 2003). The low estimations of t_s^2 found in this paper and also by other authors are also consistent

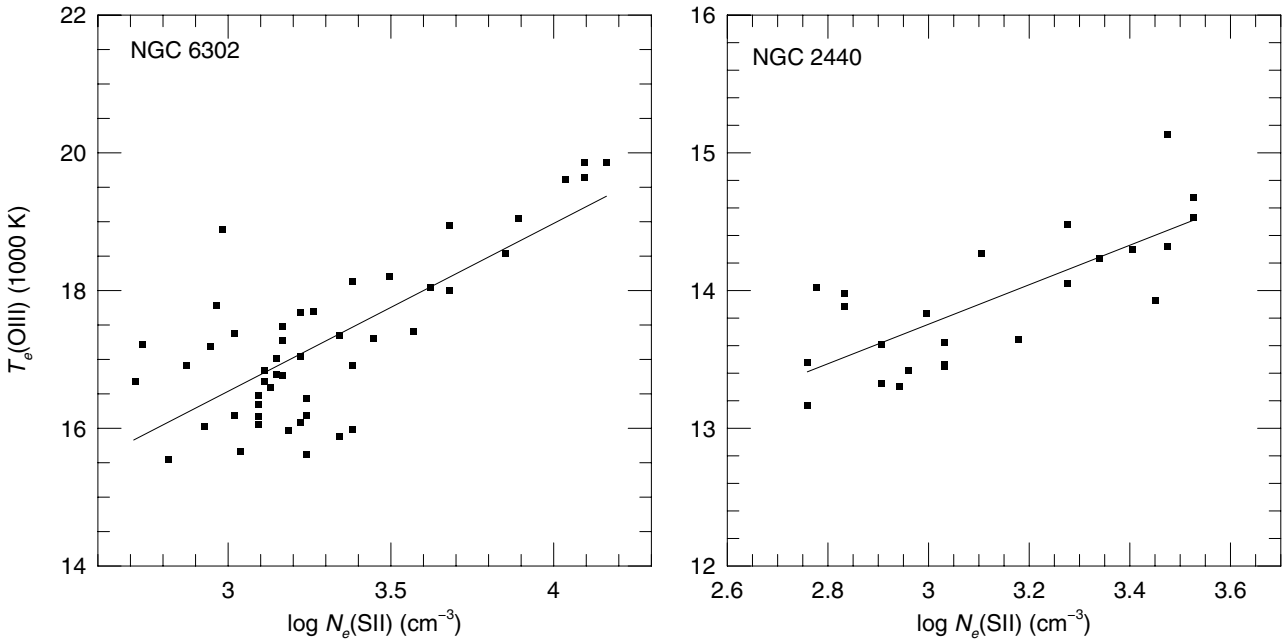

Fig. 29. T_e(O III) vs. logN_e(S II) for NGC 2440 and NGC 6302. The data analyzed for these two objects are limited to the bright regions of the nebulae, where the correlation between temperature and density can be observed.

Table 5. Electron temperature fluctuations.

Object	t_s^2(Bal)	t_s^2(N II)	t_s^2(O III)
NGC 1535	0.0003		0.0027
NGC 2438		0.0003	0.0032
NGC 2440	0.0078	0.0041	0.0011
NGC 3132		0.0006	0.0047
NGC 3242	0.0034		0.0015
NGC 6302		0.0097	0.0050
NGC 6563		0.0005	
NGC 6781		0.0021	
NGC 6853		0.0016	
NGC 7009	0.0008	0.0011	0.0023

with those obtained from photoionization models (Kingdon 1995; Gruenwald & Viegas 1995), but are too small to have a significant impact on the determination of abundance ratios derived from collisionally excited lines.

The difference found between mean [O III] and Balmer electron temperature also indicates considerable temperature fluctuations in NGC 1535, NGC 3242, and NGC 7009, and on the other hand, it indicates a low amplitude of temperature variations in NGC 2440. We have derived t^2 values from the expressions given by Peimbert (1967) relating [O III] and Balmer temperatures as a function of T_0 and t^2, assuming the same values for T_0 and t^2 in the H^+ and O^{++} zones, and we have found $t^2 = 0.0523$ for NGC 1535, $t^2 = 0.0085$ for NGC 2440, $t^2 = 0.0564$ for NGC 3242, and $t^2 = 0.050$ for NGC 7009.

Some evidences against the presence of high temperature fluctuations were presented by Liu et al. (2000). They have derived abundances of metals in the planetary nebula NGC 6153 from infrared emission lines, which are almost independent of temperature. Since these abundances were very similar to those derived from ultraviolet and optical forbidden lines, Liu et al. (2000) have rejected the presence of large temperature fluctuations in NGC 6153 and pointed out the presence of hydrogen deficient clumps within the nebula, where the heavy element recombination lines would be strongly enhanced, as a possible cause of the discrepancies between abundances derived from recombination and forbidden lines. On other hand, Ruiz et al. (2003) and Peimbert et al. (2004) have supported the hypothesis of high temperature variations in gaseous nebulae and some evidences pointed out by them are: the large differences between the Balmer and [O III] temperatures found in gaseous nebulae (Peimbert 1971; Liu & Danziger 1993; Zhang et al. 2004) and the differences of the He^+/H^+ values derived from different helium lines under the assumption of a constant electron temperature (Peimbert et al. 2004; Peimbert et al. 1995), indicating the presence of high temperature variations. Other potential evidence in favor of high temperature fluctuations was presented by O'Dell et al. (2003). These authors measured the [O III] electron temperature in 1.5×10^6 different positions in the Orion Nebula based on data obtained with the Hubble Space Telescope and they found that t_s^2(O III) = 0.008. From this value and some geometrical considerations they estimated $t^2 = 0.028 \pm 0.006$.

Although we have found temperature fluctuations of low amplitude for the planetary nebulae of our sample, we cannot completely rule out the existence of larger temperature fluctuations. As our measurements of electron temperature are averages along the lines of sight, t_s^2 is an inferior limit of t^2 and higher values of electron temperature fluctuations can possibly exist in these nebulae.

6. Conclusions

An observational study on the variation of electron temperature and density has been conducted in 10 galactic planetary nebulae, using long slit spectrophotometry of high signal-to-noise ratio in the range of 3100 to 6900 Å. Electron temperatures were determined from the [O III](λ4959 + λ5007)/λ4363 and [N II](λ6548 + λ6583)/λ5755 ratios and the Balmer discontinuity and electron densities were estimated from the [S II]λ6716/λ6731, [Cl III]λ5517/λ5537, and [Ar IV]λ4711/λ4740 ratios. The main findings are the following:

1. The electron temperature estimates obtained from [O III](λ4959 + λ5007)/λ4363 and [N II](λ6548 + λ6583)/λ5755 ratios and observed Balmer discontinuity present systematic variation along the nebular surface in most of the objects studied (NGC 1535, NGC 2438, NGC 2440, NGC 3132, NGC 3242, NGC 6302, and NGC 7009). In most of the cases, the electron temperature decreases from the center to the edges, with higher temperatures also found at the outskirts of the nebulae. For NGC 6563, NGC 6781, and NGC 6853 a uniform distribution of electron temperature have been observed.
2. Electron temperature fluctuations of low amplitude have been observed in the planetary nebulae studied here. The temperature distribution across each nebula presents a variance relative to the mean corresponding to $0.0003 \leq t_s^2(\mathrm{Bal}) \leq 0.0078$, $0.0003 \leq t_s^2(\mathrm{N\,II}) \leq 0.0097$, and $0.0011 \leq t_s^2(\mathrm{O\,III}) \leq 0.0050$. Although we have found temperature fluctuations of low amplitude for these nebulae, we cannot completely rule out the existence of larger temperature fluctuations. As our measurements of electron temperature are averages along the lines of sight, t_s^2 is an inferior limit of t^2 and higher electron temperature fluctuations can possibly exist in these nebulae.
3. A systematic spatial variation of electron density has been detected in most of objects studied. For NGC 2438, NGC 3132, and NGC 6563, the density profile presents a double peaked distribution along the nebular surface. For NGC 1535, NGC 2440, NGC 3242, NGC 6302, and NGC 7009 the electron density is decreasing from the center to the edges. The remaining objects (NGC 6781 and NGC 6853) have not shown any significant electron density dependence on position. NGC 2438, NGC 6563, NGC 6781, and NGC 6853 are in general the most diffuse and probably evolved objects studied here, with low mean densities in the range $N_e(\mathrm{S\,II}) \approx 95$–$158\,\mathrm{cm}^{-3}$.
4. An anti-correlation between temperature and density was found for NGC 2438 and NGC 3132, with the electron temperature increasing with the decrease of electron density and a correlation between temperature and density was found for NGC 1535, NGC 2440, NGC 3242, NGC 6302, and NGC 7009, with the electron temperature increasing with the increase of electron density. These relationships seem to be associated with the morphology of the nebula. The nebulae in which the correlation between temperature and density is present are ring shaped. The anti-correlation between temperature and density is found in bipolar planetary nebulae that are denser in the centre of the nebula.

Acknowledgements. This paper is based on observations made with the 1.52 m and 1.60 m telescope, obtained at the ESO and LNA, respectively. We are grateful to the Brazilian institutions CAPES, CNPQ and LNA for the partially supporting this work.

References

Aller, L. H. 1941, ApJ, 93, 236
Aller, L. H., & Walker, M. F. 1965, ApJ, 141, 1318
Aller, L. H., Ross, J. E., O'Mara, B. J., & Keys, C. D. 1981, MNRAS, 197, 95
Baessgen, M., Diesch, C., & Grewing, M. 1990, ApJ, 237, 201
Barker, T. 1983, ApJ, 267, 630
Barker, T. 1984, ApJ, 284, 589
Benjamin, B. A., Skillman, E. D., & Smits, D. P. 1999, ApJ, 514, 307
Bernard Salas, J., Pottasch, S. R., Beintema, D. A., & Wesselius, P. R. 2001, A&A, 367, 949
Boeshaar, G. O. 1974, ApJ, 187, 283
Bowen, I. S. 1960, ApJ, 132, 1
Butler, K., & Zeippen, C. J. 1989, A&A, 208, 337
Cahn, J. H., & Kaler, J. B. 1971, ApJS, 22, 319
Cahn, J. H., Kaler, J. B., & Stanghellini, L. 1992, A&AS, 94, 399
Chu, Y., Jacoby, G. H., & Arendt, R. 1987, ApJS, 64, 529
Czyzak, S. J., & Aller, L. H. 1979, MNRAS, 188, 229
Esteban, C., Peimbert, M., Torres-Peimbert, S., & Rodríguez, M. 1999, Rev. Mex. Astron. Astrofis., 35, 65
Garnett, D. R, & Dinerstein, H. L. 2001, ApJ, 558, 145
Giuliani, J. L. 1981, ApJ, 245, 90
Gonçalves, D. R., Corradi, R. L. M., Mampaso, A., & Perinotto, M. 2003, ApJ, 597, 975
Guerrero, M. A., Manchado, A., & Chu, Y.-H. 1997, ApJ, 487, 328
Guerrero, M. A., & Manchado, A. 1999, ApJ, 522, 378
Gum, C. S. 1955, Mem. R. Astron. Soc., 67, 155
Gutierrez-Moreno, A., Cortes, G., & Moreno, H. 1985, PASP, 97, 397
Gruenwald, R., & Viegas, S. M. 1995, A&A, 303, 535
Hawley, S. A., & Miller, J. S. 1978, PASP, 90, 39
Hyung, S., & Aller, L. H. 1998, PASP, 110, 466
Hummer, D. G., Storey, P. J. 1987, MNRAS, 224, 801
Juguet, J. L., Louise, R., Macron, A., & Pascoli, G. 1988, A&A, 205, 267
Kaler, J. B. 1986, ApJ, 308, 322
Kaufman, V., & Sugar, J. 1986, JPCRD, 15, 321
Keenan, F. P., Hibbert, A., Ojha, P. C., & Conlon, E. S. 1993, Phys. Scr. A, 48, 129
Kingdon, J. B., & Ferland, G. J. 1995, ApJ, 450, 691
Krabbe, A. C., & Copetti, M. V. F. 2002, A&A, 387, 29
Lennon, D. J., & Burke, V. M. 1994, A&AS, 103, 273
Liu, X.-W. 1998, MNRAS, 295, 699
Liu, X.-W., & Danziger, I. J. 1993, MNRAS, 263, 256
Liu, X.-W., Storey, P. J., Barlow, M. J., & Clegg, R. E. S. 1995, MNRAS, 272, 369
Liu, X.-W., Storey, P. J., Danziger, I. J., Cohen, M., & Bryce, M. 2000, MNRAS, 312, 585
Liu, X.-W., Luo, S.-G., Barlow, M. J., Danziger, I. J., & Storey, P. J. 2001, MNRAS, 327, 141
Liu, Y., Liu, X.-W., Luo, S.-G., & Barlow, M. J. 2004, MNRAS, 353, 1231
Maciel, W. J., & Pottasch, S. R. 1980, A&A, 88 1
Mavromatakis, F., Papamastorakis, J., & Paleologou, E. V. 2001, A&A, 374, 280

Meatheringham, S. J., Wood, P. R., & Faulkner, D. J. 1988, ApJ, 334, 862
Mendoza, C. 1983, Planetary Nebulae, IAU Symp., 103, 143
Mendoza, C., & Zeippen, C. J. 1982, MNRAS, 198,127
Minkowski, R., & Aller, L. H. 1956, ApJ, 124, 93
Moore, C. E. 1985, Selected Tables of Atomic Spectra, NSRDS-NBS 3, Sect. 11
O'Dell, C. R., Peimbert, M., & Peimbert, A. 2003, AJ, 125, 2590
Osterbrock, D. E. 1989, Astrophysics of Gaseous Nebulae and Active Galactic Nuclei, University Science Books, Mill Valley, CA
Peimbert, M. 1967, ApJ, 150, 825
Peimbert, M. 1971, Bol. Obs. Tonantzintla Tacubaya, 6, 29
Peimbert, M. 1978, Planetary Nebulae, IAU Symp., 76, 215
Peimbert, M., & Torres-Peimbert, S. 1983, Planetary Nebulae, IAU Symp., 103, 233
Peimbert, M., & Torres-Peimbert, S. 1987, Rev. Mex. Astron. Astrofis., 14, 540
Peimbert, M., Torres-Peimbert, S., & Luridiana, V. 1995, Rev. Mex. Astron. Astrofis., 31, 131
Peimbert, M., Peimbert, A., Ruiz, M. T., & Esteban, C. 2004, ApJS, 150, 431
Perek, L., & Kohoutek, L. 1967, Acad. Publ. House Czech. Acad. Sci., 1, 1
Pottasch, S. R. 1983, Planetary Nebulae, IAU Symp., 103, 391
Ramsbottom, C. A., Bell, K. L., & Stafford, R. P. 1996, ADNDT, 63, 57
Rola, C., & Pelat, D. 1994, A&A, 287, 676
Rowlands, N., Houck, J. R., Herter, T., Gull, G. E., & Skrutskie, M. F. 1989, ApJ, 341, 901
Rubin, R. H., Bhatt, N. J., Dufour, R. J., et al. 2002, MNRAS, 334, 777
Rubin, R. H., Martin, P. G., Dufour, R. J., et al. 2003, MNRAS, 340, 362
Ruiz, M. T., Peimbert, A., Peimbert, M., & Esteban, C. 2003, ApJ, 595, 247
Savage, B. D., & Mathis, J. S. 1979, ARA&A, 17, 73
Shields, G. A., Aller, L. H., Keyes, C. D., & Czyak, S. J. 1981, ApJ, 248, 569
Stanghellini, L., & Kaler, J. B. 1989, ApJ, 343, 811
Torres-Peimbert, S., & Peimbert, M. 1977, Rev. Mex. Astron. Astrofis., 2, 181
Verner D. A., Verner, E. M., & Ferland, G. J. 1996, ADNDT, 64, 1
Zeippen, C. J., Le Bourlot, J., & Butler, K. 1987, A&A, 188, 251
Zhang, Y., Liu, X.-W., Wesson, R., et al. 2004, MNRAS, 351, 935
Walter, D. K., Dufour, R. J., & Hester, J. J. 1992, ApJ, 397, 196
Weinberger, R. 1989, A&AS, 78, 301
Wiese, W. L., Fuhr, J. R., & Deters, T. M. 1996, JPCRD, Monograph, 7
Williams, R. E., & Livio, M 1995, Proc. STScI, 8, 24

Online Material

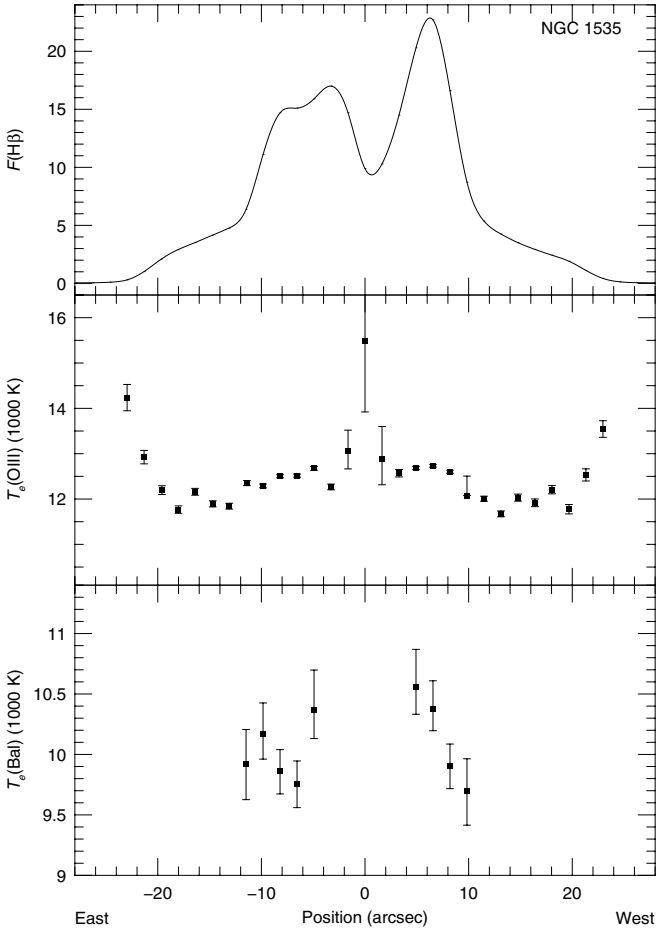

Fig. 5. NGC 1535. Spatial profiles of Hβ flux (in units of 10^{-14} erg cm^{-2} s^{-1}), $T_{\rm e}$(O III) and $T_{\rm e}$(Bal).

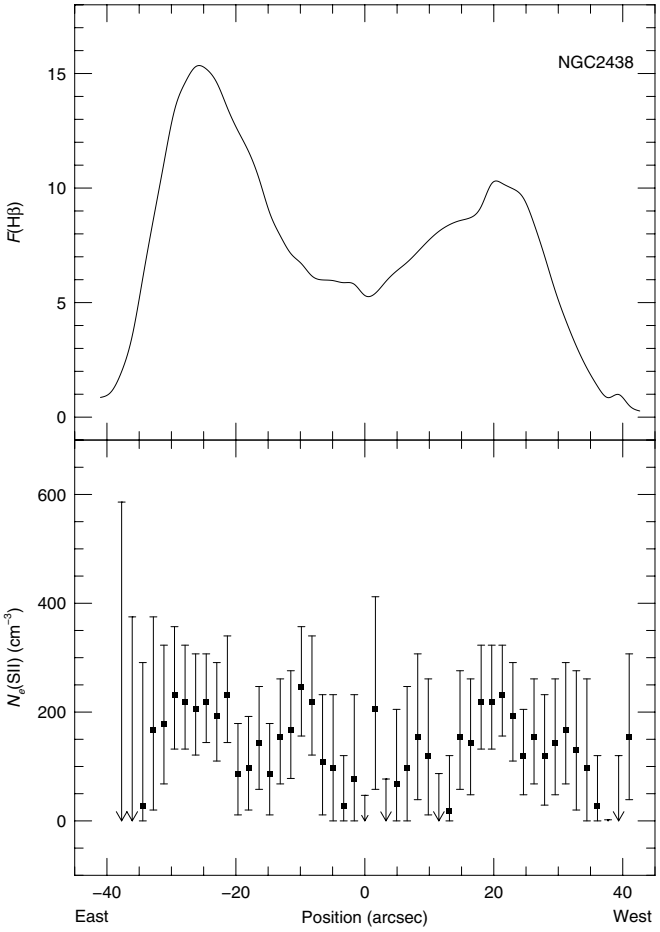

Fig. 6. NGC 2438. Spatial profiles of Hβ flux (in units of 10^{-15} erg cm^{-2} s^{-1}) and $N_{\rm e}$(S II).

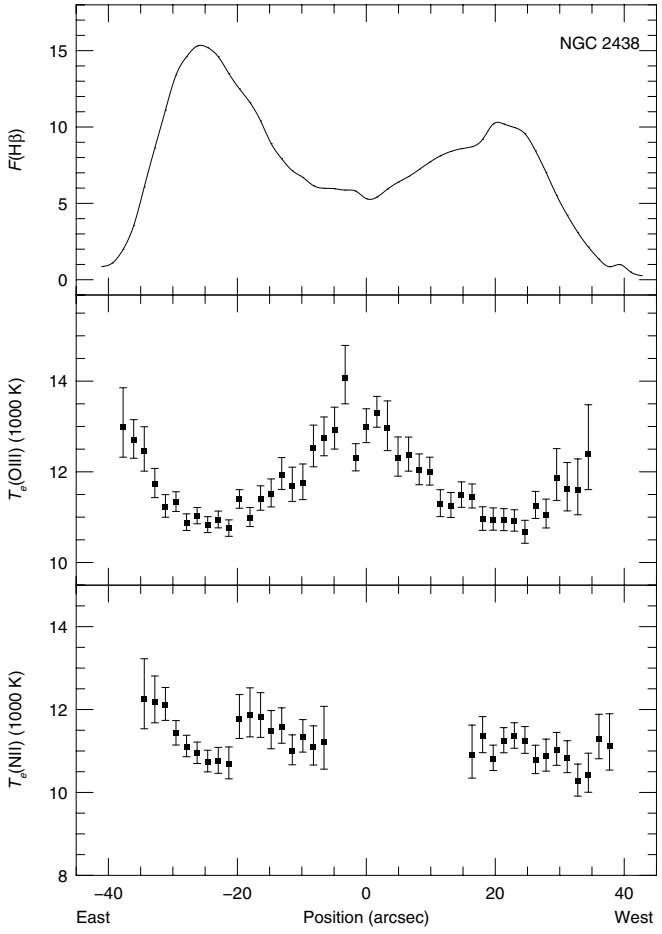

Fig. 7. NGC 2438. Spatial profiles of Hβ flux (in units of 10^{-15} erg cm^{-2} s^{-1}), T_e(O III) and T_e(N II).

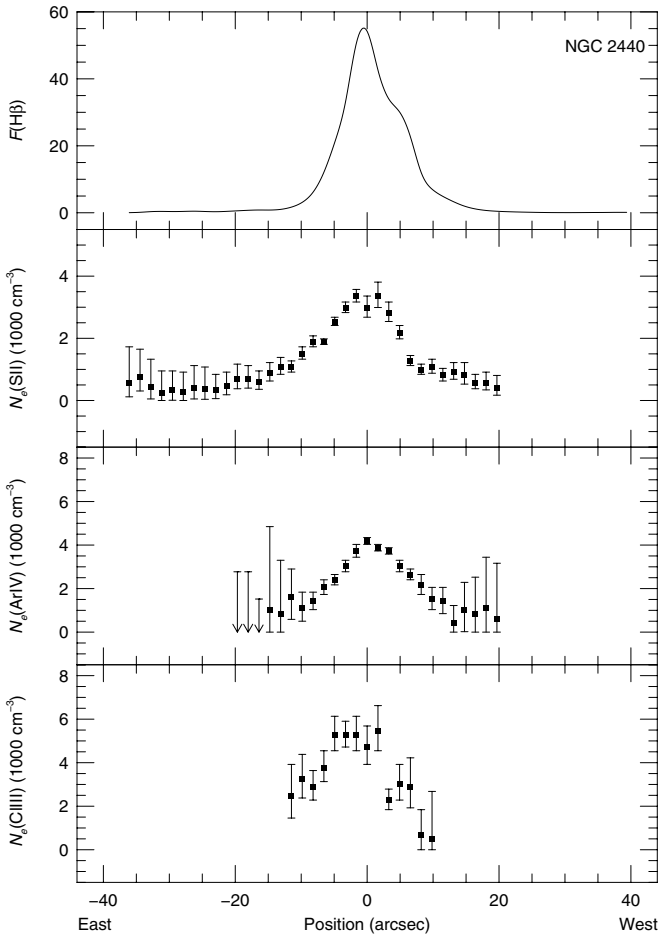

Fig. 8. NGC 2440. Spatial profiles of Hβ flux (in units of 10^{-14} erg cm^{-2} s^{-1}), N_e(S II), N_e(Cl III) and N_e(Ar IV).

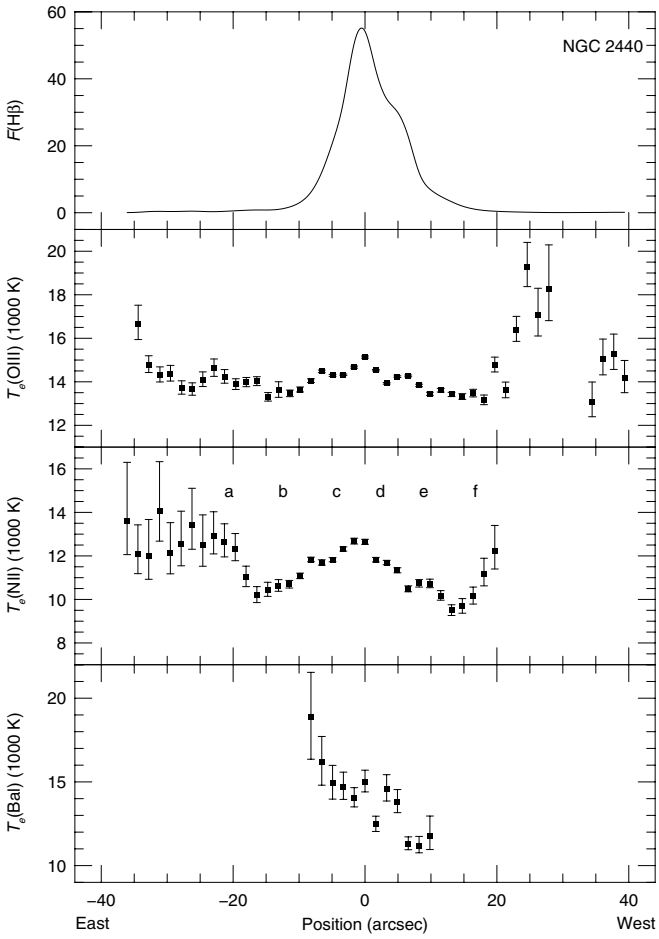

Fig. 9. NGC 2440. Spatial profiles of Hβ flux (in units of 10^{-14} erg cm^{-2} s^{-1}), T_e(O III), T_e(N II) and T_e(Bal).

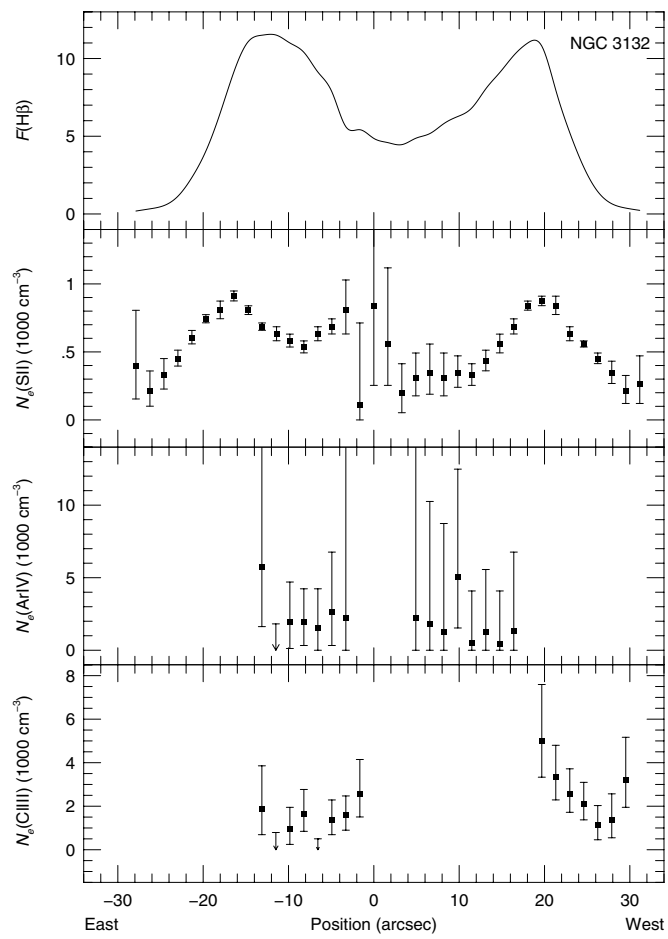

Fig. 10. NGC 3132. Spatial profiles of Hβ flux (in units of 10^{-14} erg cm^{-2} s^{-1}), N_e(S II), N_e(Cl III) and N_e(Ar IV).

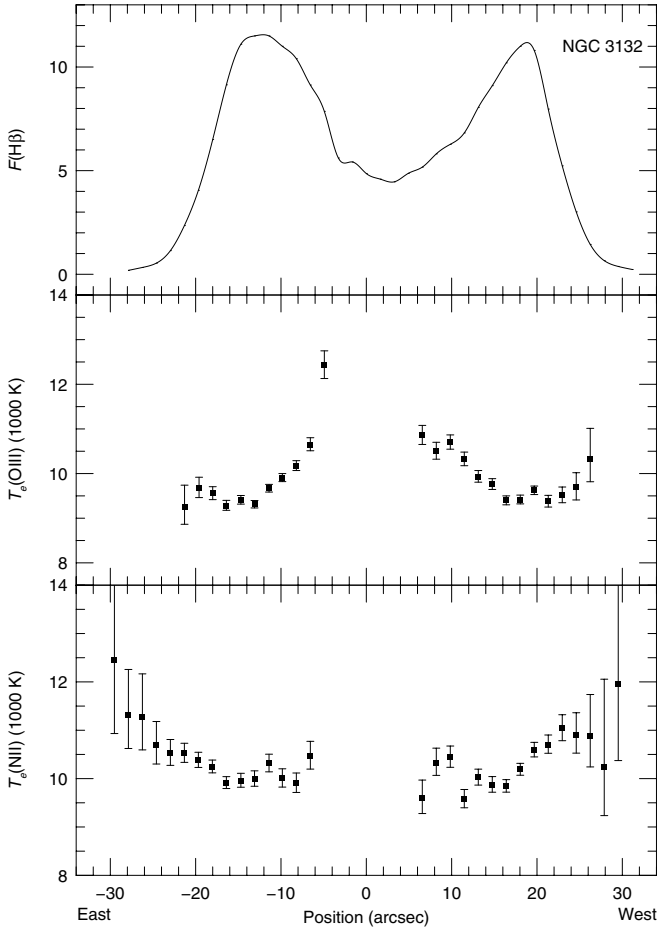

Fig. 11. NGC 3132. Spatial profiles of Hβ flux (in units of 10^{-14} erg cm^{-2} s^{-1}), T_e(O III) and T_e(N II).

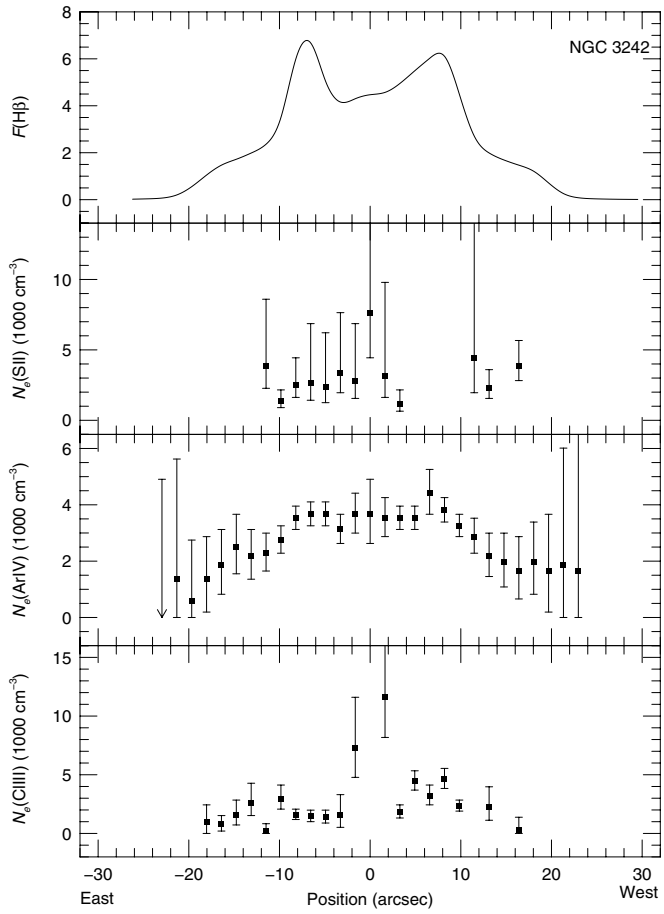

Fig. 12. NGC 3242. Spatial profiles of Hβ flux (in units of 10^{-13} erg cm^{-2} s^{-1}), N_e(S II), N_e(Cl III) and N_e(Ar IV).

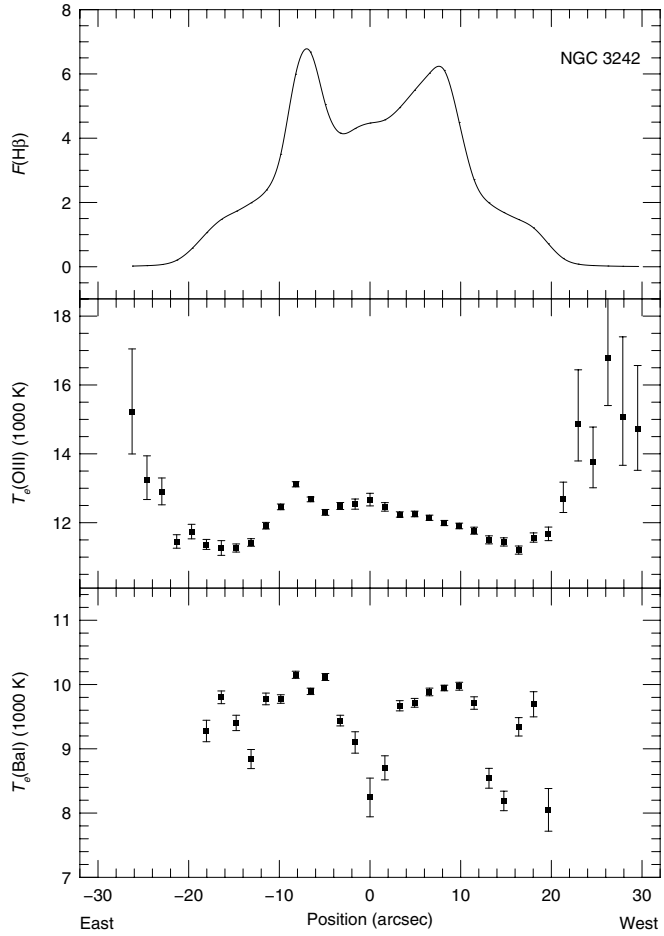

Fig. 13. NGC 3242. Spatial profiles of Hβ flux (in units of 10^{-13} erg cm^{-2} s^{-1}), T_e(O III) and T_e(Bal).

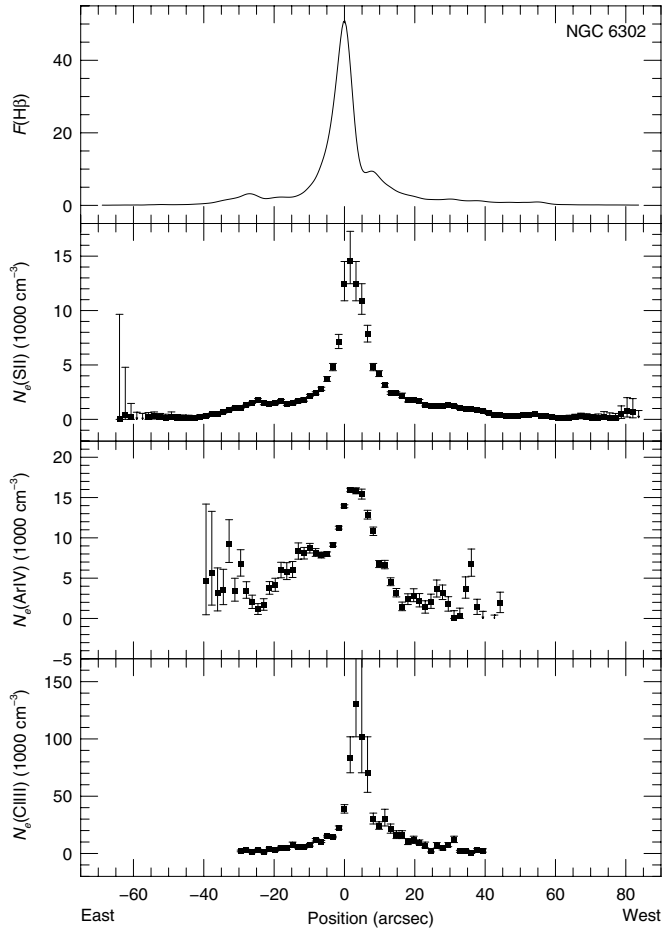

Fig. 14. NGC 6302. Spatial profiles of Hβ flux (in units of 10^{-14} erg cm^{-2} s^{-1}), N_e(S II), N_e(Ar IV) and N_e(Cl III).

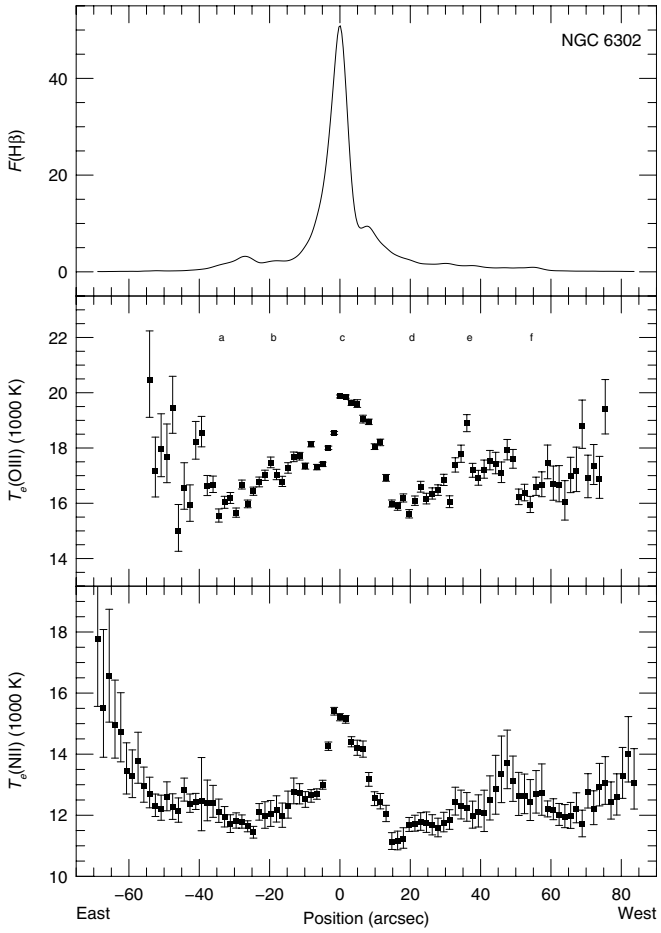

Fig. 15. NGC 6302. Spatial profiles of Hβ flux (in units of 10^{-14} erg cm^{-2} s^{-1}), T_e(O III) and T_e(N II).

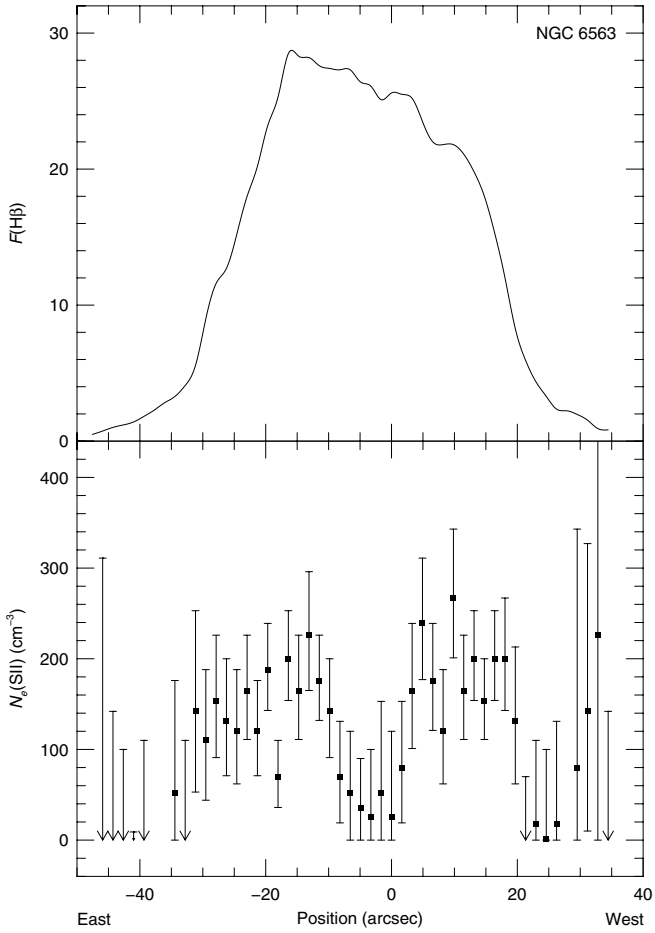

Fig. 16. NGC 6563. Spatial profiles of Hβ flux (in units of 10^{-15} erg cm^{-2} s^{-1}) and N_e(S II).

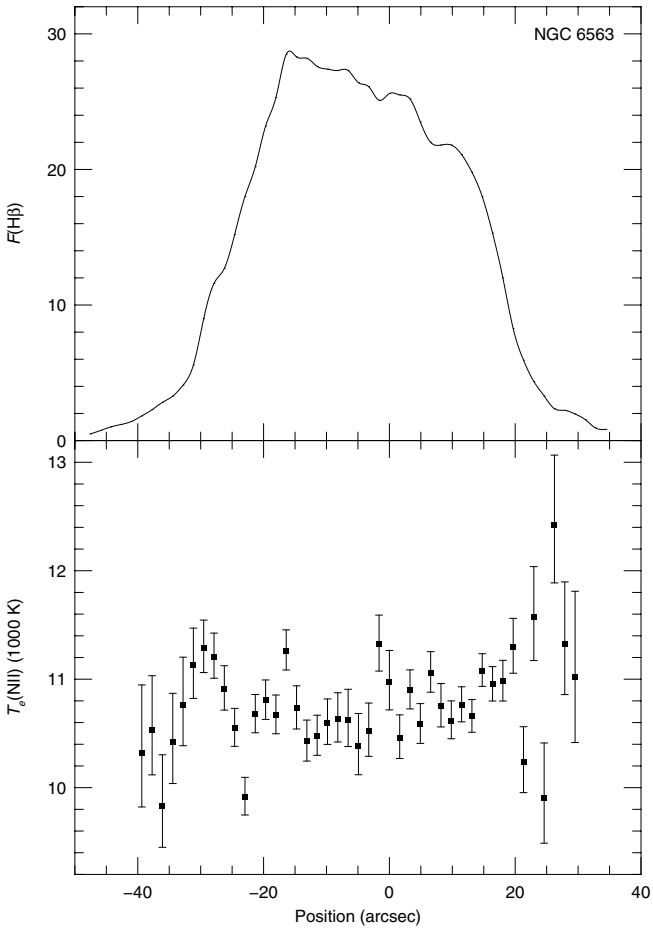

Fig. 17. NGC 6563. Spatial profiles of Hβ flux (in units of 10^{-15} erg cm^{-2} s^{-1}) and T_e(N II).

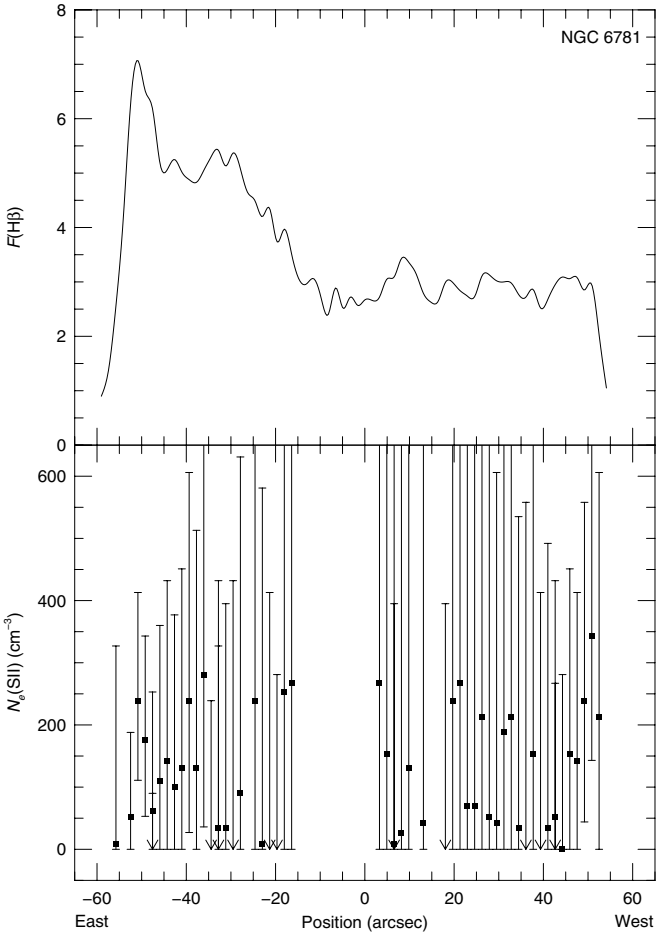

Fig. 18. NGC 6781. Spatial profiles of Hβ flux (in units of 10^{-15} erg cm^{-2} s^{-1}) and N_e(S II).

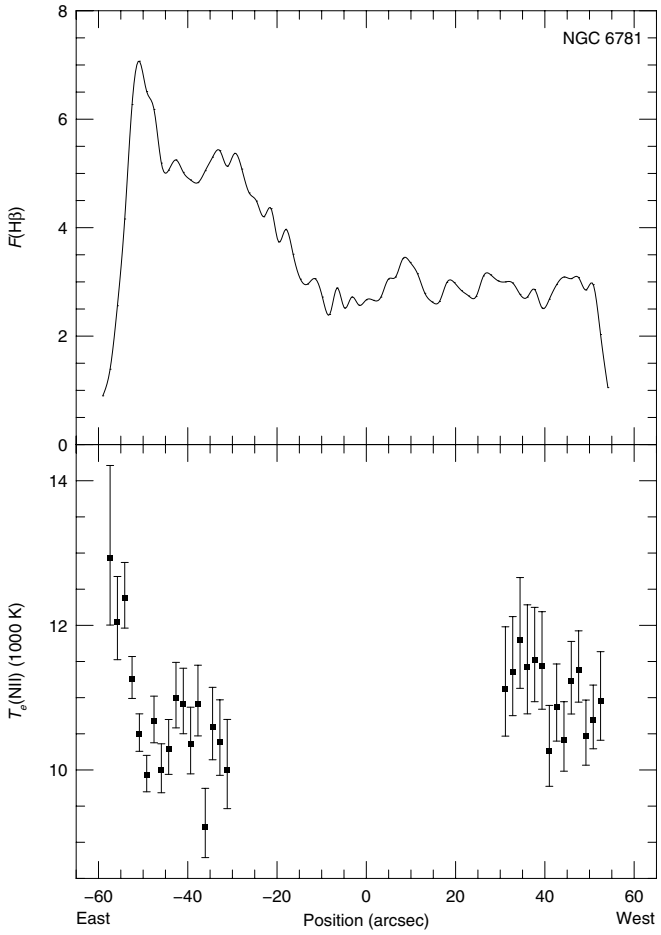

Fig. 19. NGC 6781. Spatial profiles of Hβ flux (in units of 10^{-15} erg cm^{-2} s^{-1}) and T_e(N II).

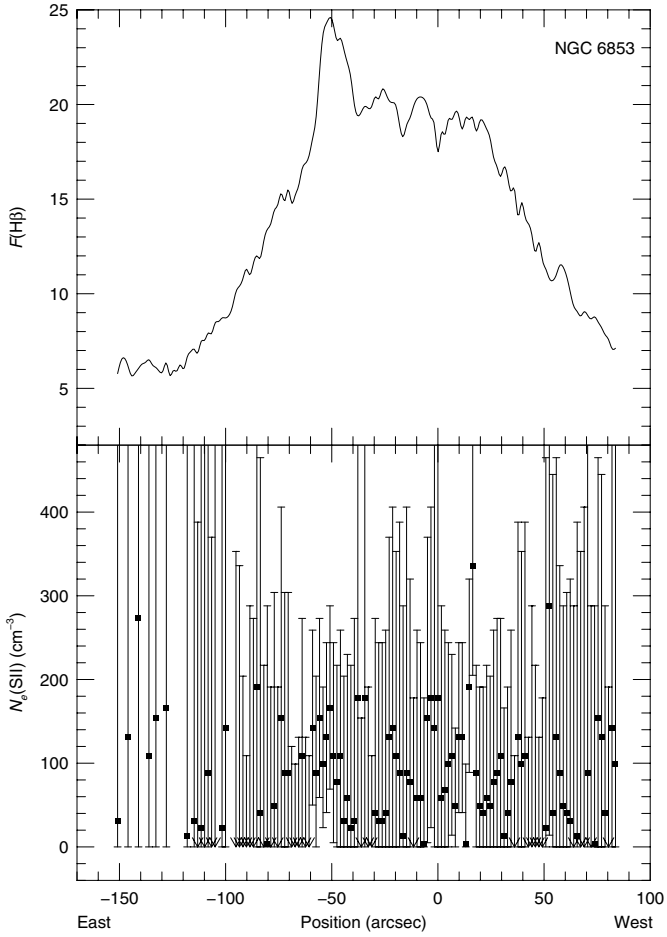

Fig. 20. NGC 6853. Spatial profiles of Hβ flux (in units of 10^{-15} erg cm^{-2} s^{-1}) and N_e(S II).

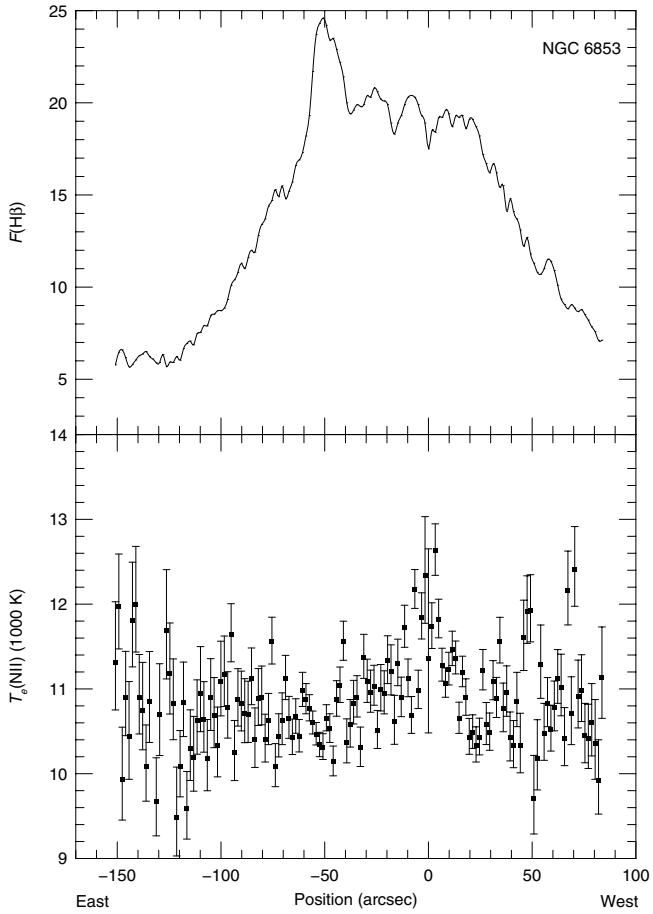

Fig. 21. NGC 6853. Spatial profiles of Hβ flux (in units of 10^{-15} erg cm^{-2} s^{-1}) and T_e(N II).

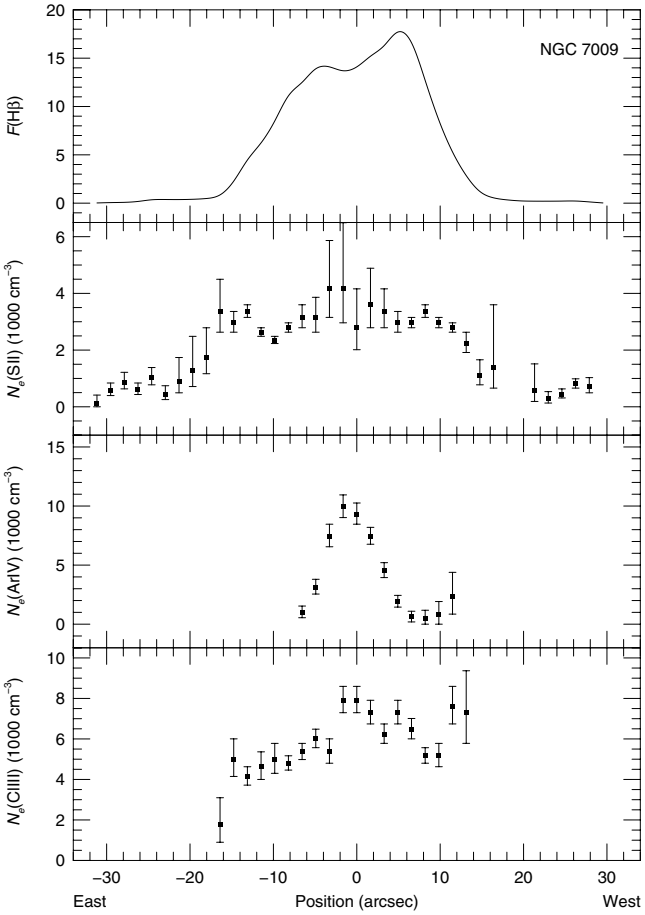

Fig. 22. NGC 7009. Spatial profiles of Hβ flux (in units of 10^{-13} erg cm^{-2} s^{-1}) and N_e(S II), N_e(Ar IV) and N_e(S II).

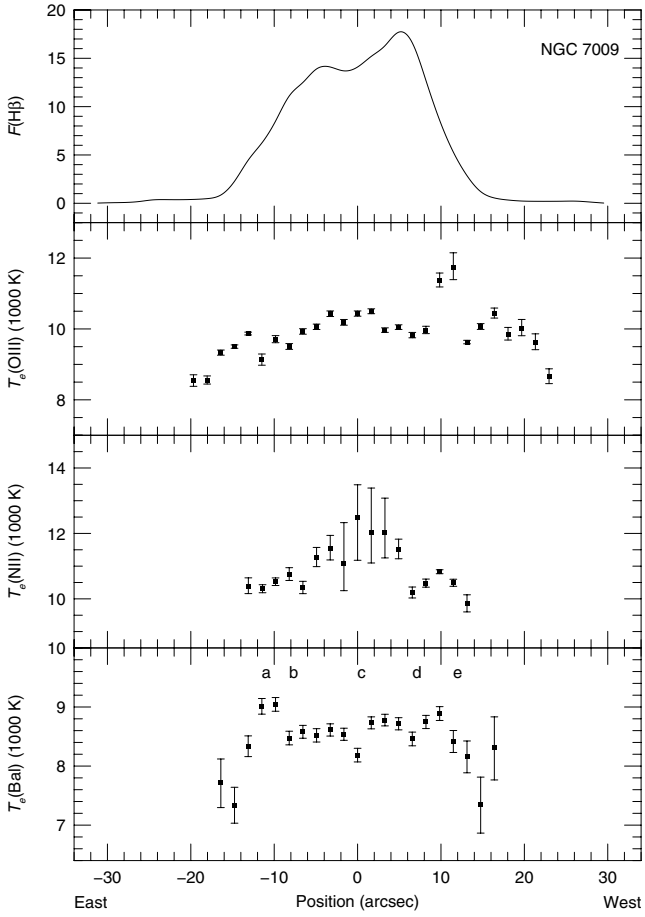

Fig. 23. NGC 7009. Spatial profiles of Hβ flux (in units of 10^{-13} erg cm^{-2} s^{-1}), T_e(O III), T_e(N II) and T_e(Bal).